An application of hierarchical Bayesian modeling to better constrain the chronologies of Upper Paleolithic archaeological cultures in France between ca. 32,000–21,000 calibrated years before present

William E. Banks, Pascal Bertran, Sylvain Ducasse, Laurent Klaric, Philippe Lanos, Caroline Renard, Miriam Mesa

An application of hierarchical Bayesian modeling to better constrain the chronologies of Upper Paleolithic archaeological cultures in France between ca. 32,000–21,000 calibrated years before present

William E. Banks [a, b, *], Pascal Bertran [a, c], Sylvain Ducasse [a], Laurent Klaric [d], Philippe Lanos [e], Caroline Renard [f], Miriam Mesa [a]

[a] CNRS, UMR 5199 – De la Préhistoire à l'Actuel: Culture, Environnement et Anthropologie, Université de Bordeaux, Allée Geoffroy Saint Hilaire, CS 50023, 33615 Pessac Cedex, France.

[b] Biodiversity Institute, University of Kansas, Lawrence, KS 66045-7562.

[c] INRAP, Centre de Recherches Archéologiques, 140 avenue Maréchal Leclerc, CS 50036, 33323 Bègles Cedex, France.

[d] CNRS, UMR 7055 – Préhistoire et Technologie, Université de Paris Nanterre, 21 Allée de l'Université, 92023 Nanterre Cedex, France.

[e] CNRS, UMR 5060 – IRAMAT-CRPAA, Université Bordeaux-Montaigne and UMR 6188 Géosciences-Rennes, Université Rennes 1, Campus scientifique de Beaulieu, CS 74205, 35042 Rennes Cedex, France.

[f] CNRS, UMR 5608 – Travaux et Recherches Archéologiques sur les Cultures, les Espaces et les Sociétés, Université de Toulouse Jean Jaurès, 5 Allée Antonio Machado, 31058 Toulouse Cedex 9, France.

Keywords: Pleistocene; Paleoclimatology; Europe; Data analysis; Chronology; Hierarchical Bayesian Age-Modeling; Upper Paleolithic

Abstract

Investigations of chronology play a key role in the majority of archaeological research endeavors and are particularly pertinent to examinations of culture-environment relationships, especially during periods characterized by rapid and marked climatic variability and environmental reorganization. Rigorous evaluations of available data and robust methods are required if one wishes to reconstruct reliable chronologies, and this is especially the case when examining periods that are associated with a relatively few radiometric measurements. Such is the case for the Upper Paleolithic archaeological record documented in present-day France from 32,000 to 21,000 calibrated years BP. We take into account critically examined radiocarbon measurements from contextually secure archaeological contexts and employ a recently-developed method of Hierarchical Bayesian Modeling to reconstruct the chronology of archaeological cultures from the Middle Gravettian to the Badegoulian. The calculated chronological

intervals for each typo-technologically defined culture phase are compared to the Greenland ice core climatic record and a terrestrial paleoenvironmental record from Bergsee Lake (Southern Germany)—itself expressed in calendar years calculated with the same calibration curve employed in our age model—thereby permitting each archaeological culture to be correlated accurately with documented paleoclimatic variability.

1. Introduction

Issues of chronology are central to archaeological inquiry. This is especially the case with heuristic approaches that take into account past environmental conditions in their investigations of past cultural adaptations. The reason being that, for certain prehistoric periods, environments were rarely stable, especially at temporal scales relevant to the Upper Paleolithic archaeological record. While the mechanisms that influenced and shaped past cultural adaptations and diversity are multiple and complex, it is a generally acknowledged that hunter-gatherer cultures each operate within an environmental context and that such contexts play a role in the cultural variability that we observe archaeologically or ethnographically, although clearly to varying degrees and in conjunction with other factors (Binford, 2001; Kelly, 2013). The potential influence of environmental conditions become especially pertinent when cultural variability and cultural transitions are examined through time and across periods of documented climatic variability. Therefore, to investigate past culture-environment relationships effectively, it is critical that these examinations have robust chronological foundations.

For the region of Western Europe situated in present-day France, many archaeological cultures are minimally (few ^{14}C ages) or poorly (e.g., non-AMS ages produced decades ago, ages made on bulk samples, etc.) dated, and therefore their chronological relationships to Dansgaard-Oeschger variability remain unclear. This is especially the case for the middle phase of the Gravettian (Klaric, 2013, 2007), early phases of the Solutrean (Renard, 2011, 2010), and the initial phase of the Badegoulian (Ducasse,

2012, 2010). A number of recently completed and ongoing research projects[1] are, in part, focused on dating, using the most up-to-date methods, archaeological contexts associated with these archaeological cultures (i.e., typo-technological phases). These projects emphasize critical taphonomic and contextual evaluations of sites and their individual archaeological levels such that samples reliably associated with specific archaeological levels are dated. Such work ensures that only culturally informative radiometric ages are included in subsequent chronological evaluations.

The objective of this article is two-fold. We aim to examine, via a recently-developed method of Hierarchical Bayesian Modeling, all reliable radiocarbon age determinations from contextually secure Gravettian, Solutrean, and Badegoulian contexts in France, ca. 32–21 cal ka BP (calibrated kiloanni before present), in order to reliably determine the chronology of the different typo-technological phases that comprise each broad technocomplex and then correlate the chronological interval of each archaeological culture with documented paleoclimatic variability. Aside from facilitating examinations of culture-environment relationships, such work also serves the important purpose of establishing an initial or baseline cultural chronology from existing, reliable (in terms of both dating method and archaeological context) radiocarbon measurements with the most appropriate Bayesian methods. This practice allows one to better identify archaeological contexts that warrant additional attention in radiocarbon dating campaigns, but will also make it possible in the future to evaluate the degree to which newly produced ^{14}C measurements improve the initially constructed chronology.

1.1. Late Pleistocene climatic variability

[1] LabEx LaScArBx "IMPACT" (W. Banks, dir.)
Programme Collectif de Recherches "SaM" (S. Ducasse and C. Renard, dirs.)
Programme Collectif de Recherches "Cassegros" (S. Ducasse and J.-M. Le Tensorer, dirs.)
Programme Collectif de Recherches "Casserole" (A. Lenoble and L. Detrain, dirs.)

The hunter-gatherer populations associated with the archaeologically-defined, regionally-specific cultural phases of the major European Upper Paleolithic technocomplexes lived during a period of the Late Pleistocene marked by pronounced climatic changes. These fluctuations occurred at millennial and sub-millennial time scales (Dansgaard et al., 1993), and the temporal resolution of this climatic variability is well-established (Rasmussen et al., 2014). Stadial–interstadial cycles were broadly synchronous across Greenland, the North Atlantic, and Europe (Austin and Hibbert, 2012; Sánchez Goñi et al., 2008), although vegetation responses were regionally differentiated (Duprat-Oualid et al., 2017; Fletcher et al., 2010; Sánchez Goñi et al., 2008) and not necessarily synchronous (Lane et al., 2013, 2012). In addition to vegetation, these climatic fluctuations had pronounced effects on landscape geomorphology, particularly the development and disappearance of permafrost (Andrieux et al., 2018; Vandenberghe et al., 2014), the extension of deserts and the deposition of aeolian sediments (Antoine et al., 2003; Bertran et al., 2013; Kasse, 2002), and ungulate distributions and biomass (Rivals et al., 2017; Sommer and Nadachowski, 2006)—factors that had the potential to profoundly influence Upper Paleolithic hunter-gatherer adaptations and distributions.

1.2. Archaeological context

An archaeologist's ability to make reliable inferences related to cultural behavior is dependent on context and association. With respect to dating past human activity, associations between material culture remains and chronological data serve as a necessary foundation for any investigation that wishes to place cultural behavior in its temporal context. Without a critical assessment of the contextual reliability of chronological data, inferences pertaining to the timing of cultural events, adaptations, or changes may be misleading or incorrect (Pettitt and Zilhão, 2015). Furthermore, even if they are accurate, radiometric determinations from insecure or compromised archaeological contexts are of little value, and the recent literature contains a number of examples of archaeological interpretations being

refuted when the archaeological contexts on which they were founded were further evaluated and found to be compromised by natural formation processes, post-depositional processes, or stratigraphic misinterpretation during excavations (Bordes, 2003; Discamps et al., 2015; Ducasse et al., 2019; Klaric, 2007; Teyssandier and Zilhão, 2018; Zilhão et al., 2015). Thus, before building any chronology, the archaeological contexts of the radiometric age determinations to be used must be critically evaluated so that only ^{14}C ages with reliable archaeological associations are retained.

1.3. Radiometric data

All chronological data are not created equal. In addition to evaluations of their archeological context, radiometric measurements themselves must be critically evaluated before being included in the construction of an archaeological chronology. The most common chronological data employed in studies of the Upper Paleolithic are radiocarbon ages, and over the last 60 years an extremely large corpus of ages has been compiled and many are readily accessible in published databases (d'Errico et al., 2011; Vermeersch, 2005). However, due to the inevitable incorporation of errors in such large compilations of data, as well as the variable quality of archaeological contexts contained within them, such databases should not be used uncritically.

Data entry errors aside, there exists another important issue that must be taken into account before using such data—that issue being data quality or measurement accuracy. Well into the 1980s, relatively large samples (> 100 g) of bone or charcoal were used to obtain a ^{14}C age, and one strategy to obtain sufficient quantities of material to be dated was to combine bone or charcoal from an entire archaeological level, or a large portion of it, and measure an age from that bulk sample. Aside from the lower precision associated with beta-counting techniques commonly used in previous decades to measure residual radiocarbon activity, bulk samples invariably included materials from a number of different occupations that are likely to be separated from one another in time—this is especially the case

in palimpsest deposits which dominate Upper Paleolithic contexts (e.g., rock shelter deposits)—thus rendering the measured ^{14}C age of little or no utility for making archaeological inferences since they are composed of materials from potentially different events, even if in some cases such results appear to be coherent.

The application of Accelerator Mass Spectrometry methods to samples allowed for the calculation of ages that were more accurate and more precise than those produced via traditional counting methods. Any casual comparison of 'conventional' ages to subsequently produced AMS ages from the same archaeological contexts illustrates this pattern, and in many instances it is clear that the 'conventional' ages should be considered aberrant since they are often clear underestimations of what subsequent work and continued dating efforts have shown with more accurate methods. Continued developments, though, demonstrate that early generation AMS ages too can be problematic due to the fact that potential contaminants were not sufficiently removed. New protocols, namely Acid Base Acid (ABA) and Acid Base Oxidation-Stepped Combustion (ABOx-SC) pretreatments, were developed in the late 1990s (Bird et al., 1999) and served to improve dating accuracy by more effectively removing carbonates and humic acids from charcoal samples. Comparisons of charcoal ages produced with the two methods indicate that the two are not always equally effective and that ABA ages have a tendency to be younger than ABox-SC ages from the same sample (Haesaerts et al., 2013).

With respect to AMS dating of archaeological bone samples, recent years have seen the development of ultrafiltration protocols used to purify extracted collagen and improve dating accuracy (Higham et al., 2006). As seen with the different protocols for pre-treating charcoal samples, the ultrafiltration method is more effective at removing contaminants than simple gelatinization of extracted collagen (Higham, 2011; Marom et al., 2012). While ultrafiltration appears to produce more reliable ages, it is clear that the method is not always successful in completely removing potential contaminants (Brock et al., 2013; Marom et al., 2013). This shortcoming appears to be especially problematic when

dating archaeological materials associated with temporal contexts that approach the temporal limit of the radiocarbon method. For example, bone samples from an Aurignacian context at the Blanchard rockshelter—samples that were previously dated via ultrafiltration—were dated using a new amino acid hydroxyproline method and the amino acid ages are on the order of three thousand years older than those obtained with ultrafiltration (Bourrillon et al., 2017). Therefore, for time periods that begin to approach the temporal limits of ^{14}C dating, one must keep in mind that even ages obtained from ultrafiltered collagen are potentially inaccurate. Lastly, chronological analyses should not focus solely on employing only ultrafiltration AMS measurements because comparisons of ultrafiltration and non-ultrafiltration age determinations on collagen obtained from samples derived from a single archaeological sample demonstrated that the two methods can produce identical ages (Ducasse et al., 2014a).

1.4. Cultural chronology construction

Upper Paleolithic archaeological cultures are defined predominantly on the basis of lithic (and in some instances bone as well) material cultural assemblages that share the same, or closely derived, tool types and associated reduction sequences (chaînes opératoires) that are well-constrained in both space and time. These definitions imply that these recognizable typological and technological features and traits were transmitted and maintained within a cohesive system that a population, or populations, employed within particular cultural and environmental contexts (Clarke, 1968; d'Errico and Banks, 2013; Klaric, 2018). This is the operating assumption behind the definition of regional Upper Paleolithic archaeological cultures and their broader technocomplexes as well. As it pertains to regionally well-constrained archaeological cultures (e.g., the Middle Gravettian/Noaillian, the *raclettes*-yielding Badegoulian), there exist multiple archaeological contexts whose assemblages share common material culture traits and for which there exist multiple radiocarbon ages. When the degree of archaeological

association between radiometric age determinations and culturally coherent material culture assemblages is high, we are able to place the associated archaeological culture within a temporal context.

This initial temporal context, though, is composed of age determinations from multiple archaeological sites and is expressed as radiocarbon years before present (^{14}C BP). Since atmospheric ^{14}C concentration varies over time as a result of changes in the production rate, the calibration of radiocarbon ages to calendar dates is necessary (Reimer et al., 2013). Calibration allows one to compare age determinations from a variety of archaeological contexts with one another and, equally as important, permits the comparison of dated archaeological cultures to environmental data whose temporal ranges are typically expressed in calendar years before present. With such broad and simplistic comparisons, though, an important class of information is not fully taken into account, that being stratigraphic information. Bayesian inference provides a solution since it permits the combination of radiocarbon data with *a priori* (i.e., stratigraphic) information (Dye and Buck, 2015; Lanos and Philippe, 2018).

Before radiocarbon measurements enter the equation, the sole information that we have at our disposal pertaining to the timing of an archaeological event of interest (i.e., a human action that took place at an unknown date in the past—the event date θ) are: 1) a general temporal interval for the target study period; 2) the hypothesis that archaeological events are *a priori* uniformly distributed within the study period; 3) an ordering of archaeological events, when they have been observed in a stratified context (i.e., relative dating); and 4) in some rarer instances, information that allow us to infer duration of archaeological events or duration of hiatuses between events (e.g., geomorphological or sedimentological information). In order to improve our understanding of this *a priori* information, we perform radiocarbon measurements on materials recovered from contexts directly associated with the archaeological events of interest. These radiocarbon measurements are then linked, via a calibration

curve, to the archaeological event dates on which bear the *a priori* information listed above. Bayes theorem allows one to combine the temporal probabilistic information provided by the calibrated radiocarbon dates with the probabilistic *a priori* information that we possessed initially—i.e., the stratigraphic ordering of the now radiometrically dated archaeological events. In essence, the calibrated radiocarbon data have improved (or refined), via the properties of conditional probability, our *a priori* information such that we obtain a posterior result that provides us with a better understanding of the timing and duration of the archaeological event(s) under investigation.

It should be apparent that since Bayesian-derived age models of archaeological chronological data use stratigraphic information and relationships as priors, it is essential, as mentioned above, that dated archaeological contexts and collections be examined critically before their associated data are incorporated into a model—an uncritical use of radiometric data from sites that are characterized by artificial archaeological associations between material culture assemblages and dated samples will produce models that are, more likely than not, wrong (Discamps et al., 2015; Pettitt and Zilhão, 2015). Thus, when constructing an age-model it is important to eliminate data (e.g., ^{14}C ages) that are demonstrably aberrant on the basis of contextual problems, sampling strategies, or a chemical/physical standpoint.

1.5. Correlating radiocarbon-based cultural chronologies with climatic chronologies

Once a regional chronology that calculates the durations of successive archaeological cultures is produced, its estimated calendar age intervals must be related to chronologies of climatic changes (e.g., ice core records) if we wish to place those archaeological cultures in their associated environmental contexts. The problem encountered here is one of differing calendar age estimates. The chronology of Late Pleistocene climatic events of the northern Atlantic has been established by counting ice layers in cores obtained from the Greenland ice sheet (Rasmussen et al., 2014). These chronologies are expressed

in calendar years before present. Since the ratios of carbon isotopes are variable through time, we must use radiocarbon calibration curves (Reimer et al., 2013) to convert, via Bayesian methods, ^{14}C ages (expressed in radiocarbon years before present) to calendar dates. A complication with this endeavor relates to the fact that radiocarbon calibration curves summarize multiple, and variable, records of changing carbon isotope ratios such that the curves provide calibrations that incorporate these errors. Moreover, calibration curves are based on the tuning of ^{14}C-based marine $\delta^{18}O$ records with those from ice records, which assumes that the Polar Front moved quickly such that a warming of sea surface temperatures is coincident with a warming in Greenland. Therefore, calibrated radiocarbon dates do not necessary reflect true calendar dates accurately. An illustrative example of this is provided by Giaccio et al. (2017). In their study, new, more precise $^{40}Ar/^{39}Ar$ dates were made on samples of Campanian Ignimbrite tephra and compared to ABA and ABOx-SC ^{14}C ages obtained from burned wood recovered from within the tephra at the same locality. When compared to the new $^{40}Ar/^{39}Ar$ calendar date, along with the recalculated previous tephra dates, one notes that the weighted mean of the multiple ^{14}C measurements, when calibrated with IntCal13, is roughly 800–1400 years too young (Giaccio et al., 2017). The mean ^{14}C calendar date obtained via calibration with the IntCal09 curve is slightly better but still represents a significant underestimation (ca. 600 years). Inversely, based on a comparison of a ^{14}C tree-ring chronology to ice core ^{10}Be records, Muscheler et al. (2014) argue that calibrated radiocarbon dates, at least for the period that they examined (ca. 41 cal ka BP), overestimate calendar age estimates by roughly 1200 years. Calibrating radiocarbon ages is, thus, clearly problematic, even if there are differing findings as to whether calibrated ^{14}C dates underestimate or overestimate actual calendar dates.

In light of these problems, it is evident that, for the time being, any archaeological chronology based on calibrated radiocarbon ages must be compared to climatic records that themselves have a chronology based on calibrated ^{14}C dates derived from the same calibration curve. In this manner, one is comparing

like with like and can be assured that correlations between the time interval of specific archaeological cultures and D-O climatic variability are reliable.

2. Materials and Methods

2.1. Chronological data

For the chronological interval targeted by this study, there exists a relatively large corpus of radiometric data, primarily ^{14}C measurements, from a number of archaeological sites. In the framework of the LabEx-funded (LaScArBx) project "IMPACT", the authors of this study compiled all available ^{14}C measurements published in archaeological journals, as well as those found in the grey literature (e.g., INRAP salvage excavation reports) and the numbers of dated sites and radiocarbon ages for each technocomplex are contained in Table 1.

As was described above, however, these radiocarbon ages are heterogeneous with respect to quality and reliability (e.g., nature of the sample, method of measurement, archaeological context). As a result, parallel to the archaeostratigraphic reassessment of several key sites conducted in the frameworks of separate projects (see footnote 1), "IMPACT" project members reviewed each published site and associated ^{14}C measurements (Gravettian: L. Klaric; Solutrean: C. Renard; Badegoulian: S. Ducasse). Such work allowed team members to evaluate the integrity of each archaeological context and to identify all ages that were obtained from bulk samples, as well as those that were called out in the literature as being problematic from a chemical or physical standpoint. We retained sites that have demonstrated taphonomic integrity (for all or portions of their sequence), whose recovered lithic industries have been either described or analyzed and thus reliably assigned to an archaeological culture, and that are associated with reliable radiocarbon ages (see Section 1.3). These sites and associated ^{14}C measurements are contained in Table 2. One will note that these evaluations greatly reduced the number of sites and radiocarbon measurements retained for this analysis, with only 39% and 35%, respectively, retained for

analysis from the corpus of available data (Table 1). This disparity between the available and retained data samples serves to demonstrate: 1) the difficulty in establishing archaeological association between ^{14}C measurements and certain cultural behaviors (e.g., decorated caves, human burials without material culture remains); 2) the influence of biases introduced by non-modern excavation methods and selective sampling of recovered material culture; and 3) the influence of post-depositional processes on the Upper Paleolithic archaeological record. The difference between available ages and those that we retained for our analysis underlines the importance of placing archaeological context and association first in any chronological study.

Concerning those archaeological contexts and associated ages that were not retained, space is not sufficient to explain, on a case by case basis, the details behind their exclusion. Suffice it to say that the reasons were various and most commonly related to the fact that radiometric ages were made on materials from archaeological levels or stratigraphic units that have either been shown to be mixed or are palimpsests combining two or more archaeological cultures such that individual ages cannot be reliably attributed to any specific one. There also exist sites that have been well-excavated and well-dated, but for which the typological attribution of the recovered assemblages remains uncertain. An example is the site of Les Bossats (Ormesson) and its well-dated Gravettian component (Bodu et al., 2011), which at present is difficult to attribute to either the Early or Middle Gravettian. This difficulty is due to the typo-technological ambiguity of the recovered assemblage and a paucity of culturally attributable assemblages in the region to which it can be compared, thus making it difficult to reliably place its ^{14}C measurements into a specific cultural phase, such as those defined for southwestern France. Additionally, numerous sites were dated decades ago and many of those ages were obtained on bulk charcoal or bone samples derived from an entire level or surface. Considering what we now know with respect to site formation and post-depositional processes, it is highly probably that these bulk ages were obtained from materials associated with different cultural events and in many cases different

archaeological cultures, so none were retained. This is in addition to the fact that when compared with more recently run ages (i.e., better decontamination and more accurate counting methods), many ages (bulk or not) measured decades ago clearly underestimate the true age of the sample. In an effort to reduce the number of potentially aberrant ages in our study sample, we retained only AMS measurements. It is also not uncommon for authors to call out ^{14}C measurements that are problematic with respect to chemistry or potential contamination, and such ages were excluded from the analysis. Finally, a large number of sites excavated decades ago either have not been subjected to thorough taphonomic or contextual examinations (e.g., refitting studies, geomorphological analyses, etc.) or have lithic industries that have not been recently described or analyzed. Recent studies (Ducasse et al., 2017, 2014a; Raynal et al., 2014a) demonstrate the importance of such analyses and their archaeological implications. By incorporating into age-models ^{14}C measurements from sites that have not undergone such critical examinations, one may unwittingly include ages that do not have reliable archeological associations—i.e., ages that may not be dating the cultural occupation to which they were originally attributed. Such is the case for the newly published ages from the upper, Magdalenian levels at Laugerie-Haute Ouest (Verpoorte et al., 2019)—levels for which the material cultural industries have not been re-examined to determine precisely their typo-technological affiliations. We, therefore, excluded ages from archaeological levels or sites that have not been examined in this manner.

2.2. Modeling and Bayesian inference using ChronoModel

Although others are available (Buck et al., 1999; Jones and Nicholls, 2002; Lanos and Philippe, 2018, 2017), the most commonly used software for calibrating ^{14}C ages and constructing Bayesian age-models is OxCal (Bronk Ramsey, 2009), and it is typically employed to create age-models for a single stratigraphic sequence. With Oxcal, for a well-dated archaeological sequence, one creates a phase for each recognized archaeological level and each phase is delineated by boundaries: a start event and an end event, which

serve to temporally delineate the phase. Like the stratigraphic archaeological levels that they represent, the phases are ordered successively thereby providing probabilistic *a priori* information. Each phase then is populated with the radiocarbon measurements obtained from materials recovered from the corresponding archaeological level so that posterior date distributions can be calculated.

One shortcoming of OxCal is related to how phase boundaries are taken into consideration mathematically, and this type of start and end phase boundaries (also implemented in the BCal software package) has been discussed extensively (Buck et al., 1992; Christen, 1994; Jones and Nicholls, 2002; Litton and Buck, 1995; Naylor and Smith, 1988). In OxCal, the Naylor-Smith-Buck-Christen (NSBC) prior is defined for a group of event dates (θ_j) that are placed within a phase that is situated between two hyper-parameters—start α and end β—in the Bayesian hierarchical structure. These event dates (θ_j) within the phase are assumed to be conditionally independent from these two boundaries and uniformly distributed between them. In the absence of supplementary information, a uniform prior joint density is assigned to the couple α and β, knowing that $\alpha < \beta$. However, in so doing, the NSBC prior provokes an effect such that dates (θ_1, ..., θ_r) become concentrated (i.e., move closer to one another) *a posteriori* (Lanos and Philippe, 2018, pp. 143–144).

Furthermore, OxCal is not well-adapted to the construction of a regional cultural chronology based on ^{14}C measurements derived from multiple archaeological sequences. When using OxCal for such a purpose (Cascalheira and Bicho, 2015; Higham et al., 2014) , one must first produce age-models for individual archaeological sequences and then extract from each sequence the calculated *a posteriori* probability distributions that refer to the boundaries between archaeological levels for which one observes a transition between archaeological cultures or traditions. These *a posteriori* transition probabilities are then inserted within a single phase of a subsequent Bayesian age-model in order to estimate the end boundary for the ensemble of stratigraphic sequences. If one is examining an interval composed of multiple cultural transitions through time, then the second generation age-model would

have multiple phases that are ordered to reflect the chronological order of the cultural transitions and each phase is populated with the multiple site-specific posterior boundary probabilities for the corresponding cultural transition/termination that are derived from the age models of individual sequences. The problem with this approach is that one is populating a second generation age-model with probability distribution functions produced with the site-specific age models—in other words, one is introducing additional unknown boundaries as priors. Thus, breaking the Bayesian scheme into two separated parts is not statistically desirable.

A recently-developed Bayesian age-modeling software package, ChronoModel (Lanos and Philippe, 2018, 2017), overcomes the above-described limitations associated with OxCal (see Appendix for methodological summaries). In ChronoModel, one constructs a phase model for each individual site sequences in which each archaeological level is represented by a phase populated with individual ^{14}C measurements from that level and that are nested in 'event' models, and these phases are ordered successively to take into account stratigraphic priors. Simultaneously, these same 'event' models can be placed within a separate phase model where each phase represents a recognized archaeological culture—such that a cultural phase can contain multiple events that may be derived from a number of archaeological contexts at one or more sites—thereby permitting ChronoModel to take into account the stratigraphic priors associated with each ^{14}C event as well as the priors associated with the succession of archaeological cultures observed in a regional archaeological record when calculating the age intervals for successive or contemporaneous archaeological cultures. The advantage to this intersecting multiphase approach is three-fold: 1) one avoids the unnecessary introduction of additional priors that is unavoidable with OxCal when attempting to construct regional chronologies with data from multiple stratified sequences (see above); 2) the inclusion of stratigraphic sequences that are not dated from top to bottom is not problematic because all the individual sequences are nested within the broad cultural phase structure, which covers the entire period of interest and is associated with its own stratigraphic

constraints; and 3) one is not limited to only using ^{14}C ages from stratified sequences since age measurements from taphonomically reliable and culturally diagnostic single component contexts can be included in the cultural phase portion of the model—thus allowing one to take into account all relevant data when constructing a regional age-model of archaeological cultures. It is for these reasons that ChronoModel was chosen for this study.

We entered the retained radiocarbon measurements into ChronoModel (Lanos and Dufresne, 2019a) using the intersecting phase structure described above (Figures 1, 2, A2). The first component of the age model is composed of individual sites characterized by multiple, stratigraphically delimited archaeological levels that are contextually secure and from which reliable ^{14}C measurements have been obtained (Figured 1, A2a). Each archaeological level is defined as a phase and stratigraphic constraints of succession are placed between each phase. After our intensive examinations of archaeological context and radiocarbon age quality, we retained a total of fourteen archaeological sequences, which was reduced to thirteen when outliers were removed following the initial model run (see below). For three sites, taphonomic analyses indicate that artifacts have moved between levels, although these vertical displacements are minor. For these sites, archaeological levels that share a common lithic industry, and thus cultural attribution, were grouped together into a single phase, such that the final stratigraphic sequence was composed of these "conglomerate" phases. This is the case with Le Blot (Delvigne, 2016) and the Upper Solutrean levels at Le Cuzoul de Vers (Ducasse et al., 2014a) (see Table 2). In the case of Rochefort (Hinguant and Colleter, 2010), the nature of the site's sediments make it likely that objects have been displaced vertically between levels 4.3 and 4.2, which form the core of the site's Solutrean contexts, so these two levels were grouped into a single phase, which could only be included in the cultural phase portion of the age model.

In parallel to this set of stratified sequences, we constructed another sequence of chronologically-ordered (constrained via succession) phases (Figures 2, A2b), each of which corresponds to a defined

typo-technological tradition or archaeological culture (e.g., Recent Gravettian, Upper Solutrean, etc.). Each radiocarbon age contained in the age model's archaeological sequence component (Figure 1) is also assigned to the phase of the age model's parallel structure that corresponds to the cultural attribution of the archaeological level from which the age originated. Therefore, each ^{14}C age from a stratified sequence is represented in both components of the constructed age model. In addition to these data, each ^{14}C measurement from a single component site (e.g., Renancourt, La Contrée-Viallet) or from a site whose levels were grouped into a single phase (e.g. Rochefort, see above) is placed solely in the second phase structure of the age model in its corresponding cultural phase. The same holds true for radiocarbon measurements from a taphonomically secure level that is contained within a stratified sequence but for which the levels above and/or below it have either been post-depositionally compromised or whose cultural attributions are uncertain such that the entire sequence—or a multi-level portion of the sequence—could not be included in site-specific portion of the model (e.g., Solutré). This intersecting, multiphase structure allows one to incorporate all relevant chronological data into an age-model rather than just those radiocarbon measurements derived from stratified contexts, thereby avoiding an age-model that is based on only a subset of all available data.

The stratigraphic constraints employed in the age model are hard (i.e., non-overlapping) transitions, whereas we know that cultural transitions were not instantaneous events. This use of hard transitions is appropriate, however, considering that the chronological resolution of radiocarbon measurements for the Upper Paleolithic is sufficiently coarse (ca. 100–300 years for a single standard deviation, typically) such that we cannot precisely identify and follow the timing of cultural transitions that most likely occurred over the course of several human generations. Furthermore, this study is focused only on the French archaeological record for a period that covers roughly 10–15ka. This restricted geographic focus eliminates problems associated with erroneous correlations between potentially non-synchronous cultural transitions across a vast geographic area composed on regions separated by large distances

and/or prominent natural barriers (e.g., mountain ranges). Therefore, with these issues in mind, we deem the use of hard transitions between model phases to be appropriate. As additional radiocarbon data become available, the number of well-dated archaeological sequences will also certainly increase in number and analyses that evaluate potential regional variability in the timing of transitions between specific cultural phases within our study area may become possible. Such work could potentially serve to test our working assumption of the broad contemporaneity of individual cultural transitions for the Upper Paleolithic archaeological record of present-day France (e.g., Middle Gravettian to Recent Gravettian, Recent Gravettian to Final Gravettian, Upper Solutrean to Badegoulian, etc.), although the resolution of ^{14}C measurements would still be a potentially limiting factor in such endeavors.

We injected the retained chronological data into this age-model structure with "Age Cal. BP" as our time scale setting and our study period defined as 40–15 cal ka BP. We chose this overly large study period to ensure that we did not impose any inadvertent constraints on ChronoModel during its sampling and calculation operations. We employed the default MCMC settings, which consist of 3 chains, 1000 burn iterations, and 500 batch iterations with a maximum of 20 batches, and 100000 acquisition iterations with a thinning interval of 10 (Lanos and Dufresne, 2019b).

Once the initial model had run to completion and was checked for convergence (see Appendix for details on evaluating convergence; Fig. A3), we examined the individual posterior standard deviation statistics for each radiocarbon measurement contained in the "Log" results in order to identify outliers (see Supplementary Appendices 1 and 3). To identify these ages that had been penalized the most heavily (i.e., outliers), the Q1, Q2 (median), and Q3 quartile values for each age were plotted. This was done to determine if there existed a clear gap among the Q2 values such that ^{14}C ages with values above a certain threshold could be deemed outliers. To reduce or eliminate any possible influence they might have, identified outliers were eliminated, despite the fact that ChronoModel severely penalizes them, and a second generation of the age model was run. In instances where an outlier was the only "event"

within a phase (i.e., an individual archaeological level) in the stratified sequence component of the age model, the phase—now empty after the elimination of the outlier contained within it—was also eliminated since ChronoModel cannot function with unpopulated phases. We ran this second-generation, outlier-free model with the same Markov Chain Monte Carlo (MCMC) settings used for the initial model. The results of this second-generation model (see Supplementary Appendices 2 and 4) are interpreted below.

2.3. Detailed description of the age model's cultural phase component

The typo-technological (i.e., archaeological culture) phase portion of the age-model structure reflects our current (and imperfect) understanding of the French Upper Paleolithic's sequence of archaeological cultures and also takes into account uncertainties associated with the precise chronological relationships between certain cultural phases (Figure 2). We know, for example, that the Middle Gravettian record north of the Pyrenees is composed of two cultural phases: the Noaillian and the Rayssian (David, 1985; Klaric, 2008). The former is defined based on the presence of a diagnostic and easily recognizable tool type, the Noailles burin. The Rayssian is characterized by a lithic industry that possessed a specific type of bladelet core, originally termed the Raysse burin, geared towards the production of blanks destined to be worked into armatures (Klaric, 2017, 2007). The Rayssian phase has a more northerly geographic extension than the Noaillian, is entirely absent from the Pyrenees archaeological record, and in the regions where both are observed the Rayssian stratigraphically succeeds the Noaillian. However, this stratigraphic, and therefore chronological, succession is debated due to the presence of individual archaeological levels that contain both Noailles burins and Rayssian bladelet cores in varying frequencies, such as the different lenses that make up level 4 at Abri Pataud, as well as levels VI, V of Le Flageolet I (David, 1985; Klaric, 2007, 2003; Pottier, 2005; Rigaud et al., 2016; Touzé, 2013). These contexts, though, are all marked by geomorphological disturbances such that the co-

occurrence of these two cultural diagnostics appears to be geomorphological in nature (Klaric, 2008, 2007, 2003) and cannot unequivocally be interpreted to reflect a cultural contemporaneity of the use of these two artifact types, with a gradual transition from one to the other through time (Bosselin and Djindjian, 1994; David, 1985; Pottier, 2005), nor that their varying proportions reflect of differences in site function (Laville and Rigaud, 1973; Rigaud, 1988). Site formation processes aside, the number of radiocarbon ages associated with the Middle Gravettian record north of the Pyrenees is extremely limited (Touzé, 2013), and this number is even further reduced when the issues of site formation processes and archaeological context enter into the equation. Due to these ambiguities and the fact that these two archaeological cultures are relatively poorly dated at present making their chronological relationship to one another difficult to ascertain, we defined a phase, termed "Northern Generic Middle Gravettian", which incorporates both Noaillian and Rayssian contexts, and is placed between the "Early Gravettian" and "Recent Gravettian" phases, as is observed in the Pataud and Flageolet I sequences (David, 1985; Rigaud et al., 2016).

As mentioned above, the Middle Gravettian archaeological record of the Pyrenees does not contain Raysse bladelet cores but is instead defined solely by the presence of Noailles burins (Foucher et al., 2008). Furthermore, coarse comparisons of radiocarbon data indicate that some Pyrenees Noaillian contexts are broadly contemporaneous with the Rayssian assemblages documented to the north (Klaric, 2008, 2007; Touzé, 2013). To take this apparent contemporaneity into account, we placed a phase named "Pyrenees Middle Gravettian" parallel to the "Northern Generic Middle Gravettian" and between the "Early Gravettian" and "Recent Gravettian" phases. This operating hypothesis is based on the observation that the oldest dated Noaillian context in the Pyrenees is younger than ca. 28,000 ^{14}C BP, which post-dates the younger range of reliable ^{14}C ages associated with the Early Gravettian. This chronological placement of Pyrenees Middle Gravettian contexts (i.e., their relationship to Early

Gravettian contexts) warrants verification as archaeological contexts are evaluated and new radiocarbon measurements are obtained for these two archaeological traditions.

The Solutrean technocomplex in France is poorly dated and few reliable radiocarbons ages from such contexts are available for study. The Aurignacian V/Protosolutrean, although recognized at a handful of sites in our region of study, is only associated with reliable and contextually secure radiocarbon measurements at the site of Laugerie-Haute Ouest, and the same holds true for the Lower Solutrean (Verpoorte et al., 2019). Level 14 at the site of Peyrugues has a ^{14}C age (GifA-95474) that is consistent with those from Laugerie-Haute Ouest level D (10), but the cultural attribution of this level is uncertain because its associated lithic industry is sparse and undiagnostic. Therefore, while this age's context is stratigraphically reliable and included in the sequence portion of the model, it was excluded from the cultural phase portion of the model due to the ambiguity surrounding its cultural affiliation (Table 2). With respect to the Middle and Upper Solutrean technological traditions, some Upper Solutrean contexts (e.g., those in the Paris Basin and the Saône River Valley) lack shouldered points, which are associated solely with Upper Solutrean contexts in the southern regions of the study area. This variability renders it difficult to determine, solely on the basis of the recovered lithic industry, whether a level represents a Middle or Upper Solutrean context. Therefore, we chose to group these two typo-technological divisions into a single phase in the second portion of the age model, which is termed "Middle & Upper Solutrean".

Similarly, for the Badegoulian technological tradition, we created a single "Badegoulian" cultural phase that includes ages from Lower Badegoulian contexts (i.e., without *raclettes* but with a diagnostic Badegoulian bone/antler industry; i.e., Cuzoul de Vers, levels 27 and 22) (Ducasse, 2012, 2010; Lelouvier, 1996) along with those from Badegoulian archaeological levels containing diagnostic *raclettes*. The reason being that the initial phase has been recognized in few archaeological contexts in Southwestern

France and reliably dated only at the site of Cuzoul de Vers (Ducasse et al., 2014a) and Casserole rockshelter (Casserole project, unpublished; Lenoble and Detrain, dirs.).

Finally, in order to adequately constrain the archaeological cultures targeted by this study, a select (i.e., non-exhaustive) sample of reliable and representative ^{14}C ages from Early Gravettian and Lower Magdalenian contexts were placed in phases at the beginning and end, respectively, of the 'Cultural Phase' portion of the age model. Some of the ages in these bookend cultural phases are also contained in the site sequence portion of the model (Pataud, Taillis des Coteaux).

2.4. Comparisons to paleoclimatic chronologies

Once ^{14}C ages are calibrated and used to create an age model composed of posterior probability distributions of the temporal intervals for the targeted archaeological cultures, one can then compare these calculated calendar date intervals to paleoclimatic chronologies (e.g., Greenland ice core chronologies) in order to correlate archaeological cultural phases with climate phases (i.e., Greenland Stadials and Interstadials). However, a potential problem with this approach lies in the fact that the available radiocarbon calibration curves (Reimer et al., 2013, 2009) may underestimate or overestimate the true calendar age of a dated sample for periods for which tree-ring based calibration does not exist (Muscheler et al., 2014), thus making any conclusions reached via comparisons between calibrated ^{14}C dates and calendar age paleoclimatic chronologies potentially erroneous. Carleton and Collard (2019) point out that chronological uncertainty associated with archaeological and paleoenvironmental records can severely hinder, or render erroneous, evaluations of human-environment interactions.

In an effort to reduce correlative uncertainty and to situate more accurately archaeological cultures within their respective paleoenvironmental contexts, we compare our posterior chronological intervals not only to the Greenland ice core climatic record (Rasmussen et al., 2014), but also to a terrestrial paleoenvironmental sequence and paleoclimatic reconstruction provided by Duprat-Oualid et al. (2017)

(Figure 3). This record was recovered from Bergsee Lake in southern Germany that remained ice-free during the Last Glacial, and the paleoclimatic reconstruction is based on an analysis of pollen remains recovered from the core. The pollen analysis permits the observation of vegetation dynamics between 45 and ca. 15 cal ka BP and the identification of Greenland Interstadials as expressed by periods of low forest cover. More importantly, the sediment core was dated via 14 AMS radiocarbon ages from multiple depths, as well as the identification of the Laacher See Tephra. Duprat-Oualid and colleagues (2017) calibrated these radiocarbon ages using CLAM (Blaauw, 2010) and the IntCal13 calibration curve. Since the chronology of the Bergsee paleoclimatic sequence is expressed in calendar years calculated from the IntCal13 curve, we can rely on it to correlate our modeled archaeological cultural intervals with observed climatic and paleoenvironmental variability. However, the sedimentation rate was not constant throughout the Bergsee record because of stronger detrital inputs to the lake during cold periods (Eichhorn et al., 2017), so one must keep in mind that climate fluctuations in between tie points (i.e., ^{14}C ages) remain poorly constrained. This is particularly the case in the interval 22.5–28 cal ka BP, which contains both an interstadial (GI-2) and one of the most treeless phase of the Last Glacial within stadial GS-3. This is also the case for the oldest part of the record (older than 35 cal ka BP), where both large age uncertainties and the low number of dated samples lead to poor chronological resolution. For the chronological interval that is the focus of this study, the calibrated calendar age underestimation produced by the IntCal13 curve is minor. The mismatches observed between the Greenland and Bergsee records between 32–21 cal ka BP are generally on the order of less than 250 years, and this difference is roughly on the same order as precision errors associated with present-day AMS measurements for this portion of the Upper Paleolithic. Furthermore, one must keep in mind that maximum counting errors for the Greenland record between Greenland Stadial (GS)-5.2 (ca. 32 cal ka BP) and GS-2.1c (23 cal ka BP) range from ca. 1100 to 500 years, respectively (Rasmussen et al., 2014). Solving these issues, though, is beyond the scope of this paper. Since a close correspondence is observed between the interstadials in

the ice core event chronology and the Bergsee vegetation record back to 28 cal ka BP, both data sets are used here to investigate the relationships between Paleolithic technocomplexes and climate variations.

We also take into account the chronological intervals associated with Heinrich Events 3 and 2, which fall within our study period (Figures 3 and 4), because the iceberg discharges characteristic of these events are known to have significantly influenced North Atlantic ocean circulation and, consequently, climatic and environmental conditions over Western Europe (Fletcher et al., 2010). Our use of the term "Heinrich Event" refers to the principal period(s) of iceberg discharge, as inferred from the presence of ice-rafted debris (IRD) in marine sequences, and associated reduction or cessation of North Atlantic circulation (McManus et al., 2004), rather than the stadial periods that surround these events (referred to as Heinrich Stadials). These events are archeologically relevant because they consistently represent the intervals associated with the most rigorous environmental conditions within their parent stadials.

While the precise chronological boundaries for Heinrich Event (HE) 3 remain uncertain, numerous studies indicate that it falls within GS-5.1. Sanchez-Goñi and Harrison (2010) conclude that the stadial event (i.e., Heinrich Stadial) that encompasses HE3 is situated between Greenland Interstadial (GI)-5.2 and GI-4. This relatively large interval does not completely correspond to the calibrated dates provided in their table because the latter are based on Elliot et al.'s (2001) ^{14}C measurements, and uncertainties associated with correcting reservoir effects when calibrating radiocarbon ages from marine contexts make such calibrations problematic and potentially inaccurate. Numerous studies that examine HE-related proxies (e.g., ice-rafted debris, $\delta^{18}O$, planktonic foraminifera, pollen) and correlate them to reliable chronological frames of reference converge on a chronological interval that more precisely places HE3 within the interval between GI-5.1 and GI-4, or roughly 30–29 cal ka BP (Hemming, 2004; Lynch-Stieglitz et al., 2014; Parker et al., 2015; Sanchez Goñi et al., 2000; Turney et al., 2016). We adopt the narrower proposed interval. This Heinrich Event also potentially differs from others in that it has been concluded that it was not associated with a complete collapse of Atlantic Meridional Overturning

Circulation (Turney et al., 2016). Its impacts on terrestrial environments in Western Europe are likely to have been less severe than what is observed during HE2, which disrupted Atlantic circulation more significantly (Hughes and Gibbard, 2015), and such a pattern is observed in the Bergsee pollen data (Duprat-Oualid et al., 2017).

Heinrich Event 2 is known to have occurred during GS-3 and is interpreted to have been relatively brief in duration (Andrews and Voelker, 2018), as was its parent Stadial (Sanchez Goñi and Harrison, 2010), although determining its exact initiation and termination dates is difficult. The latter authors place the Stadial within which HE2 occurred between 26.5–24.3 cal ka BP, which is based on calibrating Elliot et al.'s (2001) radiocarbon measurements. Naughton et al. (2009) date this Stadial to ca. 24–26 cal ka BP, and they observe IRD in the MD99-2331 core during the latter half of this interval. This IRD signature corresponds closely to the calibrated date range provided by Andrews and Voelker (2018), which covers a briefer interval between roughly 25.5–24 cal ka BP and is based on Heinrich Event proxies in marine cores at the outlet of the Hudson Strait. An even briefer interval of 25–24 cal ka BP is proposed by Hemming (2004) and Parker et al. (2015). Since the iceberg discharges associated with these events had multiple origins (i.e., Laurentide, British-Irish, and Scandinavian ice sheets) and were regionally variable in their timing and frequency, we choose the intermediate range of the intervals proposed (i.e., 25.5–24 cal ka BP). This Heinrich Event is considered to be one of the most significant perturbations in the global climate system (Hughes and Gibbard, 2015).

3. Results

3.1. Age model

As described above, there exist two generations of the age model. The first model contained all of the retained ^{14}C measurements (ages). Examinations of its individual posterior standard deviations demonstrated that those ^{14}C measurements associated with a Q2 value greater than 400 were clearly

separated from those associated with lower median values. We, thus, deemed ages with a Q2 value > 400 to be outliers. These represented roughly 18 percent of the radiocarbon measurements included in the initial model (see Table 2). While this overall percentage is not extremely elevated, higher outlier percentages do characterize the early cultural phases (e.g., Pyrenees Middle Gravettian: 36%; Northern Generic Middle Gravettian: 75%), and their removal ensured that these cultural phases in the second-generation model were not dominated by aberrant ages. Outlier elimination reduced by one (Carane 3) the number of individual site sequences included in the age model and reduced by two (Le Facteur, Grotte du Renne) the number of sites with a single retained archaeological level—the latter included only in the cultural phase portion of the model. At present, it is unclear (e.g., presence of intrusive elements in the level, contamination, etc.) why all of the ages from Le Facteur are relatively young and thus flagged as outliers. The fact that the two ages from Grotte du Renne level V are outliers adds weight to one of the three hypotheses proposed to explain the presence of a few backed points (microgravettes and backed bladelets; elements not typically observed in Rayssian assemblages) in the level—that hypothesis being that this level may include intrusive elements from Recent Gravettian occupations of the site that were not recognized during excavations (Klaric, 2003). As described earlier, once outliers were eliminated, the model was run again, and the highest posterior density (HPD, 95%) event date ranges for the ^{14}C ages contained in the second-generation age model are presented in Table 2.

Table 3 contains the HPDs, from the first- and second-generation runs, for each archaeological culture contained in the model's 'phase' component. The cultural phases' temporal intervals differ only slightly between the two model generations, thereby illustrating the degree to which outliers are penalized by ChronoModel. The similarities between the two model generations' cultural phase results are also due in part to the fact that this portion of the model is composed of a relatively large number of sequential phases, and in the majority of them non-aberrant ages predominate, thereby allowing a robust posterior chronological interval to be calculated for those few phases that contained a high

number of outliers in the first generation run. One observes that the two Middle Gravettian phases are the longest in duration. The Recent Gravettian is slightly shorter in length, and the Final Gravettian is quite brief. The trend of decreasing duration continues with the Protosolutrean, which only lasts for a period of roughly 800 years. The Lower Solutrean lasts for a period of roughly 1400 years. The Middle and Upper Solutrean phases collectively last for ca. 1700 years, and since we grouped the two together it is not possible to determine when the Middle-to-Upper Solutrean transition occurred. The Badegoulian technocomplex lasts for approximately 2300 years, and the model structure employed here does not allow us to determine when the Badegoulian phase *à raclettes* begins.

3.2. Age model – paleoclimatic correlations

The cultural phases' chronological intervals (solid bars), bounded by HPDs representing the beginning and end of each interval, are depicted in Figure 3. These results are presented in conjunction with the paleoclimatic curve reconstructed from the Bergsee pollen record (Duprat-Oualid et al., 2017), as well as the $\delta\,^{18}O$ curve from the Greenland ice sheet (Rasmussen et al., 2014). Figure 4 contains the tempo plots for each cultural phase along with the Bergsee and Greenland paleoclimatic records. A tempo plot calculates the cumulative frequency of specified archaeological events (i.e., ^{14}C measurements) within a given phase using model states generated by the MCMC routine (Dye, 2016). As a consequence, a tempo plot trajectory curve generated by ChronoModel illustrates the mean number of dated events that took place prior to a given date within a cultural phase. The MCMC calculations also allow one to determine a credibility interval (error envelope)—related to the dating uncertainties associated with posterior event dates—for the mean tempo trajectory.

Comparisons between the age model results and the two paleoclimatic records show that the Middle Gravettian and Recent Gravettian both traverse multiple climatic phases. A similar pattern is likely for the Early Gravettian, although our model structure does not allow for a precise determination

of the beginning of this cultural phase because we only incorporated a sample of reliable ^{14}C ages associated with it in an effort to constrain the Middle Gravettian. On the other hand, the Final Gravettian, Aurignacian V/Protosolutrean, Lower Solutrean, and at a minimum the early portion of the Middle Solutrean are all contained within a single stadial phase, GS-3. The chronological interval covered by the phase combining the Middle and Upper Solutrean includes GI-2.2. The Badegoulian, as a whole, falls entirely within a period of stadial conditions (GS-2.1c).

Results indicate that the Pyrenees Middle Gravettian (Noaillian) appears between 32–31.125 cal ka BP, which is an interval that contains a transition from interstadial to stadial conditions (GI-5.2–GS-5.2) (Figures 3 and 4). The appearance of the Middle Gravettian in contexts north of the Pyrenees occurs slightly later around 31,500 cal BP roughly midway through GS-5.2. It is not possible to determine when the Rayssian technical tradition first appears nor when the northern expression of the Noaillian ends due to the fact that a paucity of reliably dated contexts required us to combine northern Noaillian and Rayssian contexts into a single cultural phase. Because this phase is populated with few archaeological events, there are relatively large uncertainty measures around its tempo plot (Figure 4). Roughly the latter halves of both of our Middle Gravettian phases coincide with HE3.

The transition from the Middle Gravettian to the Recent Gravettian, in both the Pyrenees and regions to the north, is roughly coincident with the end of GS-5.1 (also the termination of HE3) and the beginning of GI-4 between 29,000–28,500 cal BP (Table 3; Figures 3 and 4). The Recent Gravettian covers GI-4, GS-4, GI-3, and the initial part of GS-3, a chronological interval composed of multiple and pronounced climatic fluctuations. This same interval in the Bergsee sequence is likewise characterized by marked fluctuations in vegetation regimes.

The HPDs for the termination of the Recent Gravettian and the start of the Final Gravettian are centered at roughly 27 cal ka BP, which is situated within the early stages of GS-3, and the tempo plots (Figure 4) show that the Recent Gravettian is no longer present after 26.5 cal ka BP. The phase and

tempo plots indicate that this final phase of the Gravettian technocomplex terminates between 26–25.5 cal ka BP, which situates it entirely within a chronological interval characterized by stadial climatic conditions, although within its interval one observes relatively pronounced, abrupt, and short-lived excursions.

The appearance of the Protosolutrean covers a relatively brief interval that begins immediately prior to 26 cal ka BP. The two HPDs that bound the phase overlap with one another and the tempo plot indicates that all dated events within the phase occur prior to ca. 25.5 cal ka BP. In the Bergsee record, this date is coincident with deteriorating environmental conditions, and the same signal is seen in the Greenland isotope curve. This cultural phase occupies an interval during which signatures of ocean cooling are observed (Naughton et al., 2009) immediately prior to HE2.

The beginning of the Lower Solutrean is observed at 25.5 cal ka BP, also situated within the latter half of GS-3, and coincides with low PCA pollen scores in the Bergsee sequence indicating that this cultural transition occurred during a period of rigorous environmental conditions within HE2. The Lower Solutrean is present across an interval that sees a slight amelioration of paleoenvironmental conditions according to the Bergsee data and then a return to rigorous stadial paleoenvironmental conditions that fall within the latter portion of HE2. It is important to point out that both the Protosolutrean and Lower Solutrean phases for our region of study are populated with few radiocarbon ages that come from a single archaeological site, and this is apparent in the uncertainty measures associated with their respective tempo plots (Figure 4).

The Lower Solutrean termination and the appearance of the Middle Solutrean (i.e., the beginning of the Middle & Upper Solutrean phase), at ca. 24 cal ka BP (Figure 4), are correlated with an interval marked by an increase in the Bergsee pollen scores that represents the end of HE2 and the final portion of GS-3. The Middle & Upper Solutrean phase covers an interval that includes GI-2.2 and whose paleoenvironmental conditions were markedly less severe than those observed during the preceding

Lower Solutrean phase. For the reasons described above, our model structure does not permit a precise chronological determination of when the Upper Solutrean appears in the archaeological record.

The termination of the Middle & Upper Solutrean phase (i.e., the Upper Solutrean termination) and the appearance of the Badegoulian occur within a relatively restricted chronological interval that begins at ca. 23 cal ka BP (Figure 3) and is associated with a moderate double peak in Bergsee pollen scores (Duprat-Oualid et al., 2017). Our Badegoulian phase occupies an interval just over 2000 years in length and that correlates to the first third of GS-2.1 (Figure 4) (Renard and Ducasse, 2015). The Badegoulian therefore immediately post-dates both the observed lowest sea-level stand between ca. 24–23 cal ka BP (Thompson and Goldstein, 2006) and the age for the Laurentide ice-sheet's maximum volume (Hughes and Gibbard, 2015).

4. Discussion

The Middle Gravettian is situated within a period marked by multiple climatic phases, and during this interval one observes a trend towards a general opening of the landscape with respect to vegetation, as well as an increase in the frequency of periglacial features (Andrieux et al., 2018; Antoine et al., 2014). With the determination of this cultural phase's timing, continued and targeted technological evaluations (chaînes opératoires, lithic raw material acquisition, etc.) are needed to better characterize Noaillian Middle Gravettian assemblages, especially those north of the Pyrenees, in order to better document the range of cultural variability present during this climatically variable interval and understand more precisely Noaillian culture-environment relationships.

As for the Middle Gravettian Rayssian technical tradition, it is absent from the Pyrenees, and while it partially overlaps the geographic distribution of the Noaillian present north of the Pyrenees, it also extends well into higher latitudes (Klaric, 2017). Preliminary evaluations indicate that the Noaillian archaeological record of the Pyrenees and that of the Rayssian are associated with significantly

differentiated ecological niches (Vignoles, 2018), suggesting that the Rayssian adaptation is associated with an expansion of the exploited ecological niche. In the region of overlap, the nature of its relation to the Noaillian is debated due to the fact that at the sites of Le Flageolet I and Pataud rockshelter there are archaeological levels in which varying frequencies of both Noaillian burins and Rayssian bladelet cores and associated bladelets have been recovered—a decreasing frequency of Noaillian burins and an increasing frequency of Rayssian elements as one moves up in the stratified sequence. Since the Rayssian represents a clear technological rupture with the northern Noaillian (Klaric, 2017), we favor the hypothesis that the co-occurrence of these two cultural markers in the same archaeological level at some sites is the result of post-depositional/site formation processes, and/or excavation bias, and/or an artificial and arbitrary stratigraphic conjunction of different occupation lenses irrespective of their individual and taphonomic characteristics (Klaric, 2007, 2003; for a detailed overview of the artificial construction and subdivisions of Pataud Level 4, see Movius, 1975). Following this logic, one can postulate that in northern Aquitaine the Rayssian post-dates the Noaillian and thus occupies a latter portion of the northern Middle Gravettian phase—an interval corresponding to HE3. It is not possible, however, to make a more precise statement concerning the appearance of the Rayssian. At present, more in-depth work is needed to establish the chronological relationship between the northern Noaillian and the Rayssian. In this vein, research focused on obtaining radiocarbon ages from taphonomically reliable Noaillian and Rayssian contexts is currently underway in the framework of the IMPACT project (directed by WEB; funded by the LaScArBx Cluster of Excellence, University of Bordeaux). With the obtention of new radiocarbon measurements from multiple, contextually secure Noaillian and Rayssian contexts, it may be possible to create individual phases for each in an age model such that we can begin to understand their chronological relationship more precisely.

The technological shift between the Middle Gravettian and the Recent Gravettian is coincident with the climatic shift from HE3 to GI-4—a transition readily observed in the Bergsee record—and the Recent

Gravettian interval contains GI-3 and the early portion of GS-3. Research is ongoing, via combined technological and ecological niche modeling analyses conducted in the framework of a project funded by the Région Nouvelle-Aquitaine (GravettoNiches; WEB and LK, dirs.), with the objectives of: 1) characterizing the ecological contexts of the Recent Gravettian, along with those of the preceding Middle Gravettian; and 2) examining, within an ecological framework, the technological and adaptive changes associated with these two cultural phases. The fact that this cultural phase as well as the Middle Gravettian both traverse multiple climatic phases means that it is difficult to argue that these archaeological cultures represent adaptations to specific environmental conditions within the range of glacial landscapes.

The Final Gravettian is the first of multiple typo-technologically defined archaeological cultures situated within GS-3. Subsequently and roughly coincident with the period of ocean cooling immediately prior to HE2 one observes the Protosolutrean, and then within this Heinrich Event is the Lower Solutrean. While the chronological intervals associated with these two initial Solutrean phases should be viewed as tentative considering that they are based on few dated events from a single archaeological context (Laugerie-Haute Ouest), they are nonetheless constrained by phases (Final Gravettian, Middle & Upper Solutrean) that are relatively well-populated by dated events. Thus, their chronological intervals are unlikely to change significantly as additional radiocarbon measurements from contextually secure levels are obtained and taken into account. It is interesting that the chronological intervals established for these two initial phases of the Solutrean with our model—a model that targets a single geographically well-constrained region—correspond well to the ages of these phases from more distant regions, such as the extreme western limits of the Iberian Peninsula (Zilhão, 2013). While clearly associated with HE2, an interval characterized by especially cold, arid conditions and open environments in Western Europe (Andrieux et al., 2018; Duprat-Oualid et al., 2017; Fletcher et al., 2010), the Solutrean adaptation is also observed across a broad geographic area that was composed of diverse ecological

settings. This geographic distribution and ecological diversity indicate that one cannot reduce the appearance of the Solutrean to factors solely related to environment and subsistence. However, the establishment and maintenance of geographically broad social networks (Whallon, 2006) that would have been necessary for the rapid spread of its unique technological characteristics across Western Europe are likely indicative of a social response to the higher levels of ecological risk that would have been associated with HE2 (Banks et al., 2009; Zilhao, 2013).

Based on the stratigraphically observed relationship between the Middle Solutrean and the Upper Solutrean, it can be concluded that the Middle Solutrean begins during the final stages of HE2 towards the end of GS-3. As stated earlier, the timing of the transition between the Middle and Upper Solutrean cannot be established with our model's structure, so it is not possible to know how the timing of GI-2.2 and GI-2.1, which are situated within the duration of this composite cultural phase, relate to the appearance of the Upper Solutrean. It is reasonable to conclude that the Upper Solutrean overlaps to some degree with these interstadials. While these results show that Banks et al.'s (2009) correlation of the Middle Solutrean to HE2 is no longer entirely valid, they do demonstrate that their use of rigorous versus less rigorous paleoenvironmental variables to estimate ecological niches for the Middle and Upper Solutrean, respectively, was appropriate. Furthermore, their conclusion that milder climatic conditions during the Upper Solutrean (i.e., the latter portion of our combined phase) would have reduced ecological risk, which resulted in an observed regionalization of populations and cultural drift (Zilhao, 2013), is supported by our chronological results.

The transition to the Badegoulian falls solidly within the early portion of GS-2. While our understanding of the cultural transition between the Upper Solutrean and the Badegoulian is increasingly well-documented (Ducasse et al., 2014b) and while the recognized cultural rupture between the two traditions has been hypothesized to be the result of socio-economic influences (Renard and Ducasse, 2015), at present, the resolution of radiocarbon results is not sufficient to correlate these

cultural changes with potential environmental variability. Similarly, available data do not appear to indicate that faunal communities changed, to any significant degree, across this interval (Castel et al., 2014). Future research focused on directly dating and obtaining isotopic signatures from faunal and microfaunal remains would certainly aid to improve our comprehension of environmental conditions and dynamics during the 24-21 cal. ka BP timespan. The chronological interval for this phase is based on a relatively large number of radiocarbon measurements from a diverse set of archaeological contexts, so it is unlikely to shift to any great extent as additional ^{14}C ages are added to the model. Finally, because we decided to combine radiometric data from Lower Badegoulian (without raclettes) and typical Badegoulian (with raclettes) assemblages (see above), it is not possible to establish when the transition between the two occurred. Furthermore, the internal cultural processes and dynamics at work behind the technological developments between the Lower and Upper Badegoulian remain uncertain and are the subject of detailed, ongoing projects (see note 1), whose work includes radiometric reassessments of key archaeological sequences.

5. Conclusions

Archaeological research is based on inference, and therefore the data employed must hold up to rigorous scrutiny. One could argue that an issue common to most, if not all, investigations in our discipline is that of chronology. Therefore, when working to place archaeological phenomena into a temporal framework, the importance of working with datasets that have been intensively vetted cannot be overstated. Furthermore, Bayesian methods are founded on *a priori* knowledge, which in archaeological applications represents not only stratigraphic information but also demonstrated association between dated materials and discrete, cohesive material culture assemblages. Without such demonstrated associations for the entire sample of radiometric measurements used to populate an age model, one risks obtaining inaccurate or flawed results.

Critical evaluations of the nature of associations between material cultural assemblages and radiometric measurements can potentially result in large numbers of archaeological contexts being eliminated from inclusion in an age model. Not only are some sites eliminated from consideration entirely, but one is also confronted with situations for which only a single archaeological level at a given site is shown to be unaffected by site formation or post-depositional processes. Similarly, the archaeological record also includes single component sites that cannot be included in an age model in a methodologically reliable manner for certain Bayesian software packages. We employed ChronoModel because its statistical modeling framework allows one to construct a single age model structure that incorporates data from stratified sequences, stratified sites that possess a sole level unaffected by post-depositional processes, as well as single component sites.

For studies aimed at correlating an archaeological chronology with a paleoclimatic or paleoenvironmental chronology, it is extremely important that the two are temporally comparable. As has been demonstrated recently for European contexts (Duprat-Oualid et al., 2017; Giaccio et al., 2017), chronologies composed of calibrated radiocarbon dates are not necessarily concordant with the Greenland paleoclimatic chronology that is derived from counting ice layers, especially for periods situated towards the maximum temporal limit of the radiocarbon method. While this study concerns a period for which the mismatch between the IntCal13 curve and the Greenland chronology is relatively minor, and in fact is on the same order as the precision error of the target period's AMS ^{14}C measurements, we still think it is important to take into consideration a paleoenvironmental record that is calibrated in the same way as the archaeological chronology in order to reduce potentially erroneous correlations. Furthermore, the paleoclimatic record of Greenland does not reflect conditions that were present over Western Europe. For example, it has been shown that a strong warming in Greenland does not necessarily coincide with the same amplitude of warming in Europe (Sánchez Goñi et al., 2008). It is for these reasons that we used the Bergsee paleoenvironmental record to better correlate the intervals

of Upper Paleolithic archaeological cultural phases with paleoclimatic events and gain an understanding about what such events represent in terms of paleoenvironmental conditions in this region of Western Europe.

Finally, the cultural chronology produced by this study warrants refinement as new data, both archaeological and chronological, are obtained. This is especially the case for the Solutrean technocomplex, and all the phases of which it is composed, as well as the Middle Gravettian in regions north of the Pyrenees. The paucity of radiocarbon measurements for certain time periods necessitated the grouping of some typo-technological variants together (e.g., the northern Noaillian and the Rayssian), thereby preventing us for determining the nature of their chronological relationship. Similarly, the Protosolutrean and the Lower Solutrean have only been reliably dated in our region of study at a single archaeological site, thereby providing a non-representative view of their temporal contexts. It is hoped that as new data are incorporated into the model structure subsequent generations of results will validate those that we present.

Appendix: Overview of Methods used in ChronoModel

ChronoModel (CM) is a user-friendly Bayesian chronological modeling software package created for interpreting chronometric (e.g., radiometric) data in conjunction with detailed chronological and contextual information. It is founded on a new statistical concept for estimating the date of a target event that introduces an individual error for each chronometric date (Cassen et al., 2009; Lanos and Dufresne, 2012; Sapin et al., 2008). This approach differs from that implemented in the BCal (Buck et al., 1999) and OxCal (Bronk Ramsey, 2009) software packages.

ChronoModel is free, open-source, and cross-platform (Mac, Windows, Linux). The software is freely available for download from the ChronoModel website (https://www.chronomodel.com) where pre-compiled binaries of the latest version of the software are archived. One can also

download the source code and compile the program from scratch. CM is built on Qt5—Qt is a C++ toolkit for cross-platform application development—and uses the FFTW library (http://www.fftw.org), so to compile the package, one needs to have Qt5 installed on his/her computer. Finally, the CM project is hosted on GitHub and the repository can be cloned by typing: "https://github.com/Chronomodel/chronomodel.git".

CM presents a user-friendly interface where data can be organized into a model structure using intuitive graphical elements (thumbnails). These elements serve to explicitly illustrate the data and all prior information taken into account in the model.

The Bayesian statistical models and methods implemented in CM are documented in detail in prior publications (Lanos and Philippe, 2018, 2017), as well as an earlier version of the User's Manual (Vibet et al., 2016), which provides methodological explanations in a manner more accessible to non-specialists. The purpose of this Appendix is to provide an abbreviated overview of the statistical methods implemented in CM that are pertinent to the present study.

Temporal concepts employed in ChronoModel

ChronoModel is based on the following temporal concepts:

1) Event Date.

At the core of CM is the concept of the unknown Event date, which is defined mathematically via a hierarchical Bayesian statistical model (Fig. A1). This parameter represents the unknown calendar date (target date) θ of a temporal event within a given chronology, and in CM different types of measurements may be combined to estimate the date of the target event. Assuming that the event can reliably be associated with one or several suitable samples, on which measurements (M) have been made and calendar dates (t) obtained, the Event model combines these calendar dates, assumed to be contemporaneous, in order to estimate the unknown target date (θ) of the

event. A measurement (*M*, called "data" in CM) may be a ^{14}C (radiometric) age, a luminescence age, archeomagnetic parameters, or any Gaussian age measurement.

It is important to point out that archaeological situations in which multiple measurements can be unequivocally associated with a unique event are rare. For this study, with the exception of multiple ^{14}C measurements obtained from a single sample (artifact), the underlying assumption must be that each radiocarbon measurement represents a unique event due to site formation processes, meaning that each recognized archaeological level represents a palimpsest of an unknown number of events.

2) Phase (group of events)

In CM, a phase is represented by a group of archaeological events —defined on the basis of archaeological, historical, geological, environmental, or other criteria—that one wishes to place in time and that are represented by the target event dates θ estimated in ChronoModel (Fig. A2). Unlike the event date model, behind the concept of phase in CM is the assumption that, *a priori*, event dates are uniformly distributed in time, the temporal boundaries of which are defined by the start (*Ta*) and end (*Tb*) of the so-called 'study period' (Fig. A2b). This is due to the fact that it is difficult to determine the true rhythm with which events accrued through time. On the other hand, one can estimate the beginning, duration, and end of a phase on the basis of the posterior event dates (θ) observed within it.

3) Prior temporal information

In order to improve our knowledge of the parameters of an event date via Bayesian modeling, it is necessary to provide as much prior information as possible, and this is accomplished by linking events (when possible) and/or phases with temporal order relationships. These order relationships can be defined in different ways: stratigraphic ordering (stratigraphic relationships observed in the

field) or by changes in stylistic, technical, or architectural criteria whose development through time is known. All of these relationships operate directly on the target event dates. Consequently, in a modeling project, separate phase models (multiphasing) can be defined on the basis of different criteria such that one phase model can intersect another. In the present study, we create an ordered phase structure for each stratigraphic archaeological sequence such that each archaeological level (or grouping of levels that share the same lithic technology and that are connected by refits) in the sequence is a unique phase (Fig. 1; Fig. A2a). Within a given site sequence, each of the level phases is related to the neighboring phases with a temporal order relationship. These site-specific phase structures intersect with the phasing system constructed for the different archaeological cultures defined in France for the portion of the Upper Paleolithic that we target (Fig. 2; Fig. A2b). With this intersecting multiphase structure, an event (θ), which is estimated with an individual ^{14}C measurement, can potentially belong to a phase in one system (an archaeological level within a specific site sequence), as well as a phase in the second system (its associated archaeological culture in the cultural phase sequence). An event that comes from a single component site (i.e., a site that possesses only one cultural level), is only included in a single phase structure, that being the Cultural Phase sequence. Such a network of constraints can contribute significantly to improving the precision and reliability of the estimates. This system of intersecting phase structures is made possible by the Event date model and, for the moment, is unique to ChronoModel.

4) Outliers

Unlike the BCal and OxCal software packages, CM does not have a specific function to detect outliers. CM does not consider that some samples are outliers due to suspected contamination or due to the fact that they do not appear to date the event with which they are stratigraphically associated. In fact, in CM all dated events related to a target event can be disturbed *a priori* owing

to unknown error sources. This potential disturbance is modeled by the individual variance parameters (σ^2) within the Bayesian hierarchical framework of the event date model (Fig. A1) (Lanos and Philippe, 2017). For each measurement (*M*), CM assigns an *a priori* density distribution to each individual variance (Lanos and Philippe, 2017). As a result, the posterior distribution of the variance parameter provides a means with which to evaluate whether a specific chronometric measurement can be interpreted to be an outlier.

Data entry and age-model structure construction

We refer the reader to the ChronoModel webpage (www.chronomodel.com) for information on how to enter chronometric data (i.e., create events), group events into phases, impose temporal constraints, and perform Bayesian calculations. Detailed instructions and examples can be found in the User Manuals, which are available in the Downloads section (https://chronomodel.com/ download-chronomodel-software-mac-windows) for each released version of the software package.

Calibration of radiocarbon measurements

First, each radiocarbon measurement *M* needs to be calibrated into a calendar date *t*, which is accomplished with a calibration curve. Multiple curves are available in CM, and we used the IntCal13 curve (Reimer et al., 2013).

Numerical Calculations

In Bayesian modeling, posterior densities and their marginal densities are of interest. In general, we cannot derive posterior distributions analytically. If we use θ to represent the parameter of interest and *y* to represent the data sample, then the posterior distribution $p(\theta|y)$, is proportional to the product of the likelihood function and the prior probability distribution of θ, as follows:

$$p(\theta|y) \propto p(y|\theta)p(\theta)$$

Gibbs sampling

We can construct a sample of θ from $p(\theta|y)$ by using a numerical technique based on the Gibbs sampler. Gibbs sampling is a Markov chain Monte Carlo (MCMC) algorithm for obtaining a sequence of observations that are approximated from a specified multivariate probability distribution. This sequence can be used to approximate the joint and the marginal distributions of the variables or to compute integrals (such as the expected values and variances of the variables). The Gibbs algorithm samples from a large set of variables by sampling each variable in turn, conditional on the current values of the other variables and on the data (chronometric measurements). For each sample draw, the Metropolis–Hastings algorithm, adaptive rejection sampling, or the inversion method is used according to the type of variable (event date, chronometric date, individual variance). It can be shown that the sequence of samples obtained in this way constitutes a Markov chain (Gelfand et al., 1990; Geman and Geman, 1984) and the stationary (i.e., equilibrium) distribution of that Markov chain is the posterior joint distribution from which one can obtain the posterior marginal distributions. We refer the reader to Sections 4.2 and 4.3 of the ChronoModel v1.5 User's Manual (available at www.chronomodel.com) for detailed descriptions of the various methods used in ChronoModel for conducting MCMC calculations.

The most important issue to be evaluated is whether the MCMC simulation has reached convergence. At present, there is no feature in CM that automatically performs such an evaluation, so it is up to the user to conduct such work. To this end, there are three tools in ChronoModel that can be used for this: history plot, acceptance rate, and/or correlation between successive values. These three tools are described in detail in the ChronoModel v1.5 User Manual (available at

www.chronomodel.com). Below, we present an example concerning the use of the history plot to such end.

MCMC history plot

Figure A3 depicts an example of Markov chains history, and such plots can be inspected visually for convergence. Convergence will be indicated by a history that is marked in its latter stages by an equilibrium that differs from that observed during the starting state (burn-in period). Another means is to examine parallel Markov chains, each computed with different starting values, and therefore different seeding values. If the posterior distributions estimated by the different chains are highly similar, this indicates that equilibrium has been achieved. If equilibrium is not reached, then the number of iterations for the burn-in period should be increased (see User's Manual available online). A higher number of iterations per batch may also be necessary.

Outlier penalization

The event date model in ChronoModel allows chronometric measurements whose calibrated dates are far from the target event date or in contradiction with stratigraphy to be automatically penalized. As a result, a dedicated outlier detection method in CM is not necessary (Lanos and Philippe, 2017). One can assess the presence of an outlier by consulting the posterior individual variance (σ^2) distribution associated with the calibrated date t and the event date θ. As shown in the article, the age model containing all ^{14}C ages and the model from which likely outliers were removed both produced essentially identical results (Table 3). This is due to the robustness of the event date model when confronted with aberrant measurements or stratigraphic contradictions.

Statistical Results mentioned in the article text

For each marginal posterior density of a parameter, definitions of the statistical results are mentioned in the article are as follows:

1) Credibility interval (CI): this represents the shortest credible interval expressed at a given confidence level (generally 95%).

2) HPD region: this refers to the most likely calendar date range(s) for the parameter in question. It represents a set of intervals that have the highest posterior density at a given confidence level. In short, any year included in a reported HPD region has a higher posterior density than any year outside that region. It can be characterized either as an interval (if the density is unimodal) or as a discontinuous set (if the density is multimodal).

3) Standard deviation: this is the standard deviation of the Markov chain.

4) Q2 (Median): this is the numerical value separating the lower 50% of the data from the upper 50%. For this study, Q2 values of the Markov posterior standard deviation associated with each chronometric measurement were examined, and it was observed that a majority of these values fell under 400 with a smaller population characterized by values well above that, thus those with a value greater than 400 were considered as outliers.

Acknowledgements

The authors wish to thank André Morala and Hélène Valladas for allowing us to include the unpublished ^{14}C age from Le Callan, Audrey Lafarge for granting us permission to use the ^{14}C ages from La Contrée Viallet and Cottier. We thank Jean-Michel Geneste and Jean-Pierre Chadelle for giving us access to unpublished data from Combe Saunière, Pierre Bodu for granting access to data from the site of Les Bossats (Ormesson), as well as the Musée National de Préhistoire staff who provided access to archaeological collections. We appreciate the input of Guillaume Guérin concerning methodology, as well as the comments provided by João Zilhão, Francesco d'Errico, and María Fernanda Sánchez Goñi on an earlier version of the paper. Finally, we thank the editor and the two anonymous reviewers whose

comments served to strengthen the paper. This research was conducted within the framework of the project IMPACT (directed by WEB), which is funded by the LabEx Cluster of Excellence “LaScArBx” (ANR-10-LABX-52).

Table Captions

Table 1: Number of inventoried sites and ^{14}C measurements by typo-technological phase. The number of sites and ^{14}C ages retained for analysis after critical evaluations of both site contexts and individual age measurements are contained in columns four and five. The last column concerns the number of ages retained for the second generation model following the elimination of identified outliers. † We did not retain ^{14}C measurements made on human remains that are not associated directly with diagnostic material culture remains (e.g., the sites of Cussac, Vilhonneur), nor from decorated caves since it is difficult to associate ages from such contexts with material remains when they are present. While sites and/or levels deemed to be taphonomically unreliable were excluded from consideration, we did retain ^{14}C measurements from diagnostic Badegoulian antler or bone manufacturing debris from the sites of Pégourié and Rond-du-Barry.

Table 2: List of ^{14}C measurements retained for inclusion in the age-model. The unmodeled calibrated (IntCal13) Highest Posterior Density (HPD) is provided for each age as is the Posterior (i.e., modeled) event date HPD. Those ^{14}C ages that were identified to be outliers are indicated and do not have Posterior event date HPDs since they were not included in the final version of the model. Age measurements in italics and marked with an asterisk (*) are those that are included in the site sequence portion of the model but not in its cultural phase component. †† We did not retain ^{14}C measurements made on human remains that are not associated directly with diagnostic material culture remains (e.g., the sites of Cussac, Vilhonneur), nor from decorated caves since it is difficult to associate ages from such contexts with material remains when they are present. While sites and/or levels deemed to be

taphonomically unreliable were excluded from consideration, we did retain ^{14}C measurements from diagnostic Badegoulian antler or bone manufacturing debris from the sites of Pégourié and Rond-du-Barry.

Table 3: Modeled intervals (calibrated calendar years BP; IntCal13) for individual typo-technological phases in the second component of the age model structure for generation 1 (all ^{14}C ages) and generation 2 (minus outliers). The beginning of the Early Gravettian and the end of the Lower Magdalenian are in italics and marked with an asterisk (*) because these two typo-technological phases were populated with a non-exhaustive sample of radiocarbon measurements in order to reliably constrain the cultural phases targeted in this study.

Figure Captions

Figure 1: Age model component composed of individual stratified sequences (second generation model without outliers) for which each phase represents an archaeological level, or combined levels, characterized by a typo-technologically diagnostic material culture assemblage. Each phase (level) is populated with its associated dated events (^{14}C measurements). Stratigraphic relationships between phases are indicated with black lines.

Figure 2: Age model component composed of cultural (typo-technological) phases. Each phase is populated with the ^{14}C ages from the individual and culturally (typo-technologically) attributable site levels that make up the stratified sequence component of the age model. Some phases also contain ^{14}C ages from single component sites or isolated intact levels, which could not be included in the site sequence portion of the model. Chronological relationships, based on stratigraphic relationships observed in the archaeological record, between phases are indicated with black arrows.

Figure 3: Phase interval results for each typo-technological (cultural) phase produced in the age model from which outliers were excluded (second generation). a) Modeled chronological intervals for the examined typo-technological phases. The solid bars depict the shortest intervals within which fall the beginning and the end of a phase at a 95% confidence level. Posterior distributions (95%) for the beginning (dotted) and end (dashed) of each phase are also depicted. b) Bergsee principal component analysis (PCA) axis 1 scores (Duprat-Oualid et al., 2017) for the target study period. c) NGRIP $\delta^{18}O$ record (Rasmussen et al., 2014). The chronological intervals for Heinrich Events (HE) 3 and 2 used in this study (see text) are depicted in blue. The blue-dashed interval immediately preceding HE2 represents a period of ocean cooling (Naughton et al., 2009). Greenland Interstadials are indicated in grey.

Figure 4: Tempo plot results for each typo-technological (cultural) phase produced in the age model run (second generation) from which outliers were excluded. a) Each tempo plot represents a calculation of the cumulative frequency of event dates within the phase such that it illustrates the mean number of dated events that took place prior to a given date. Credibility (stepped lines) and Gaussian error (dashed lines) envelopes, both derived from the MCMC calculations, are depicted. b) Bergsee principal component analysis (PCA) axis 1 scores (Duprat-Oualid et al., 2017) for the target study period. c) NGRIP $\delta^{18}O$ record (Rasmussen et al., 2014). The chronological intervals for Heinrich Events (HE) 3 and 2 used in this study (see text) are depicted in blue. The blue-dashed interval immediately preceding HE2 represents a period of ocean cooling (Naughton et al., 2009). Greenland Interstadials are indicated in grey.

Figure A1: Figure A1: Direct Acyclic Graph (DAG) for the hierarchical model of a set of *r* event dates θ_j. Chronometric dates t_{ji} are assumed to be contemporaneous to the event date θ_j. The experimental variance s^2_{ji} of each measurement M_{ji} is evaluated by the laboratory during the measurement process. The inclusion of individual error effects σ^2_{ji} is motivated by the fact that each measurement can be affected by irreducible errors (Lanos & Philippe, 2017) related to sampling

procedures, sample handling, laboratory preparation, and/or other uncontrollable random factors. This hierarchical Bayesian model automatically penalizes outliers. It is important to note that arrows represent the direction of causality, which is opposite the direction of archaeological inference.

Figure A2: Schematic illustrating how Event Dates are contained within the different phase models. For the site sequence phase models (a), each phase represents an observed archaeological level, and the different colors represent a typo-technological (archaeological culture) attribution, the exception being Phase C3 in grey. The < symbol represents stratigraphic succession with phases to the left being older (stratigraphically below) those to the right. The Multiphase (intersecting) model (b) is composed of a succession of phases, each representing a unique typo-technological tradition (i.e., archaeological culture). Each phase is populated with event dates, and associated priors, from all archaeological contexts attributed to its corresponding typo-technological tradition. The arrows between cultural phases represent the temporal succession of archaeological cultures observed in a regional archaeological record. These multi-phase ordering constraints act on the event dates and are taken into account during the MCMC sampling.

Figure A3: Example of a history plot (also called a trace) showing the values (vertical scale) sampled during the MCMC process, which here is comprised of more than 12000 iterations. The values of the burn-in period (green) are rejected, as are the values of the adaptation process (grey) that corresponds to the Metropolis-Hastings algorithm tuning. The values of the acquisition process (blue), have reached a stationary state and consequently may be used to construct the posterior distribution of the parameter of interest (e.g., the event date). The red line represents the mean of the values sampled during the acquisition process. The green error bars associated with the red line represent the standard deviation of this mean. Note: the data used in this example are unrelated to the present study but were chosen because the associated history plot illustrates well the concerned processes.

References Cited

Allard, M., 2011. Habitats gravettiens sous l'abri des Peyrugues (Orniac, Lot) entre 25000 BP et 22000 BP, in: Goutas, N., Klaric, L., Pesesse, D., Guillermin, P. (Eds.), À La Recherche Des Identités Gravettiennes: Actualités, Questionnements, Perspectives, Memoire de La SPF. Société préhistorique française, Paris, pp. 359–372.

Allard, M., Chalard, P., Jeannet, M., Juillard, F., Le Gall, O., Pommies, M.P., Alix, P., Goupil, S., Jarry, M., 1996. Les Peyrugues (Orniac, Lot). Rapport de Synthèse, Fouille Programmée 1994–1996. SRA Midi-Pyrénées, Toulouse.

Andrews, J.T., Voelker, A.H.L., 2018. "Heinrich events" (& sediments): A history of terminology and recommendations for future usage. Quat. Sci. Rev. 187, 31–40. https://doi.org/10.1016/j.quascirev.2018.03.017

Andrieux, E., Bateman, M.D., Bertran, P., 2018. The chronology of Late Pleistocene thermal contraction cracking derived from sand wedge OSL dating in central and southern France. Glob. Planet. Change 162, 84–100. https://doi.org/10.1016/j.gloplacha.2018.01.012

Antoine, P., Catt, J., Lautridou, J.-P., Sommé, J., 2003. The loess and coversands of northern France and southern England. J. Quat. Sci. 18, 309–318. https://doi.org/10.1002/jqs.750

Antoine, P., Goval, E., Jamet, G., Coutard, S., Moine, O., Hérisson, D., Auguste, P., Guérin, G., Lagroix, F., Schmidt, E., Robert, V., Debenham, N., Meszner, S., Bahain, J.-J., 2014. Les séquences loessiques pléistocène supérieur d'Havrincourt (Pas-de-Calais, France) : stratigraphie, paléoenvironnements, géochronologie et occupations paléolithiques. Quaternaire 25, 321–368. https://doi.org/10.4000/quaternaire.7278

Aubry, T., Walter, B., Peyrouse, J.-B., 2014. Paléolithique moyen et Supérieur de la Vallée de la Claise : Bilan de vingt ans d'étude et nouvelles perspectives. Bull. Amis Mus. Préhistoire Gd.-Press. 65, 9–29.

Austin, W.E.N., Hibbert, F.D., 2012. Tracing time in the ocean: a brief review of chronological constraints (60–8 kyr) on North Atlantic marine event-based stratigraphies. Quat. Sci. Rev., The Integration of Ice core, Marine and Terrestrial records of the last termination (INTIMATE) 60,000 to 8000 BP 36, 28–37. https://doi.org/10.1016/j.quascirev.2012.01.015

BANADORA, 2018. Banque Nationale de Données Radiocarbone : pour l'Europe et le Proche Orient.

Banks, W.E., Zilhão, J., d'Errico, F., Kageyama, M., Sima, A., Ronchitelli, A., 2009. Investigating links between ecology and bifacial tool types in Western Europe during the Last Glacial Maximum. J. Archaeol. Sci. 36, 2853–2867. https://doi.org/10.1016/j.jas.2009.09.014

Barshay-Szmidt, C., Costamagno, S., Henry-Gambier, D., Laroulandie, V., Pétillon, J.-M., Boudadi-Maligne, M., Kuntz, D., Langlais, M., Mallye, J.-B., 2016. New extensive focused AMS 14C dating of the Middle and Upper Magdalenian of the western Aquitaine/Pyrenean region of France (ca. 19–14 ka cal BP): Proposing a new model for its chronological phases and for the timing of occupation. Quat. Int. 414, 62–91. https://doi.org/10.1016/j.quaint.2015.12.073

Bazile, F., 2006. Datations du site de Fontgrasse (Vers-Pont-Du-Gard, Gard.) Implications sur la phase ancienne du Magdalénien en France Méditerranéenne. Bull. Société Préhistorique Fr. 103, 597–602. https://doi.org/10.3406/bspf.2006.13475

Bertran, P., Sitzia, L., Banks, W.E., Bateman, M.D., Demars, P.-Y., Hernandez, M., Lenoir, M., Mercier, N., Prodeo, F., 2013. The Landes de Gascogne (southwest France): periglacial desert and cultural frontier during the Palaeolithic. J. Archaeol. Sci. 40, 2274–2285. https://doi.org/10.1016/j.jas.2013.01.012

Binford, L.R., 2001. Constructing Frames of Reference: An Analytical Method for Archaeological Theory Building Using Ethnographic and Environmental Data Sets. University of California Press, Berkeley.

Bird, M.I., Ayliffe, L.K., Fifield, L.K., Turney, C.S.M., Cresswell, R.G., Barrows, T.T., David, B., 1999. Radiocarbon Dating of "Old" Charcoal Using a Wet Oxidation, Stepped-Combustion Procedure. Radiocarbon 41, 127–140. https://doi.org/10.1017/S0033822200019482

Blaauw, M., 2010. Methods and code for 'classical' age-modelling of radiocarbon sequences. Quat. Geochronol. 5, 512–518. https://doi.org/10.1016/j.quageo.2010.01.002

Bodu, P., Bignon, O., Dumarçay, G., 2011. Le gisement des Bossats à Ormesson, région de Nemours (Seine-et-Marne): un site gravettien à faune dans le Bassin parisien, in: Goutas, N., Klaric, L., Pesesse, D., Guillermin, P. (Eds.), À La Recherche Des Identités Gravettiennes : Actualités, Questionnements, Perspectives, Memoire de La SPF. Société Préhistorique Française, Paris, pp. 259–272.

Bodu, P., Dumarçay, G., Naton, H.-G., 2014. Un nouveau gisement solutréen en Île-de-France, le site des Bossats à Ormesson (Seine-et-Marne). Bull. Société Préhistorique Fr. 111, 225–254. https://doi.org/10.3406/bspf.2014.14396

Bordes, J.-G., 2003. Lithic taphonomy of the Châtelperronian/Aurignacian interstratifications in Roc de Combe and Le Piage (Lot, France), in: Zilhão, J., D'Errico, F. (Eds.), The Chronology of the Aurignacian and of the Transitional Technocomplexes: Dating, Stratigraphies, Cultural Implications, Trabalhos de Arqueologia. Instituto Português de Arqueologia, Lisbon, pp. 223–244.

Bosselin, B., Djindjian, F., 1994. La chronologie du Gravettien français. Préhistoire Eur. 6, 77–115.

Bourrillon, R., White, R., Tartar, E., Chiotti, L., Mensan, R., Clark, A., Castel, J.-C., Cretin, C., Higham, T., Morala, A., Ranlett, S., Sisk, M., Devièse, T., Comeskey, D.J., 2017. A new Aurignacian engraving from Abri Blanchard, France: Implications for understanding Aurignacian graphic expression in Western and Central Europe. Quat. Int. https://doi.org/10.1016/j.quaint.2016.09.063

Brock, F., Geoghegan, V., Thomas, B., Jurkschat, K., Higham, T.F.G., 2013. Analysis of Bone "Collagen" Extraction Products for Radiocarbon Dating. Radiocarbon 55, 445–463.

Bronk Ramsey, C., 2009. Bayesian Analysis of Radiocarbon Dates. Radiocarbon 51, 337–360. https://doi.org/10.2458/rc.v51i1.3494

Buck, C.E., Christen, J.A., James, G.N., 1999. BCal: an on-line Bayesian radiocarbon calibration tool. Internet Archaeol. 7.

Buck, C.E., Litton, C.D., Smith, A.F.M., 1992. Calibration of radiocarbon results pertaining to related archaeological events. J. Archaeol. Sci. 19, 497–512. https://doi.org/10.1016/0305-4403(92)90025-X

Carleton, W.C., Collard, M., 2019. Recent Major Themes and Research Areas in the Study of Human-Environment Interaction in Prehistory. Environ. Archaeol. 0, 1–17. https://doi.org/10.1080/14614103.2018.1560932

Cascalheira, J., Bicho, N., 2015. On the Chronological Structure of the Solutrean in Southern Iberia. PLoS ONE 10, e0137308. https://doi.org/10.1371/journal.pone.0137308

Cassen, S., Lanos, P., Dufresne, P., Oberlin, C., Delqué-Kolic, E., Le Goffic, M., 2009. Datations sur site (tables des marchands, alignement du grand menhir, er grah) et modélisation chronologique du néolithique morbihannais, in: Cassen, S. (Ed.), Autour de La Table. Explorations Archéologiques et Discours Savants Sur Des Architectures Néolithiques à Locmariaquer, Morbihan (Table Des Marchands et Grand Menhir). CNRS and University of Nantes, Nantes, pp. 737–768.

Castel, J.-C., Boudadi-Maligne, M., Ducasse, S., Renard, C., Chauvière, F.-X., Kuntz, D., Mallye, J.-B., 2014. Animal Exploitation Strategies in Eastern Aquitaine (France) during the Last Glacial Maximum, in: Foulds, F., Drinkall, H., Perri, A., Clinnick, D., Walker, J. (Eds.), Wild Things. Recent Advances in Palaeolithic and Mesolithic Research. Oxbow Books, Oxford, pp. 160–174.

Christen, J.A., 1994. Summarizing a Set of Radiocarbon Determinations: A Robust Approach. J. R. Stat. Soc. Ser. C Appl. Stat. 43, 489–503. https://doi.org/10.2307/2986273

Clarke, D.L., 1968. Analytical Archaeology. Methuen, London.

d'Errico, F., Banks, W.E., 2013. Identifying Mechanisms behind Middle Paleolithic and Middle Stone Age Cultural Trajectories. Curr. Anthropol. 54, S371–S387.
d'Errico, F., Banks, W.E., Vanhaeren, M., Laroulandie, V., Langlais, M., 2011. PACEA Geo-Referenced Radiocarbon Database. PaleoAnthropology 2011, 1–12.
Dansgaard, W., Johnsen, S.J., Clausen, H.B., Dahl-Jensen, D., Gundestrup, N.S., Hammer, C.U., Hvidberg, C.S., Steffensen, J.P., Sveinbjörnsdottir, A.E., Jouzel, J., Bond, G., 1993. Evidence for general instability of past climate from a 250-kyr ice-core record. Nature 364, 218–220. https://doi.org/10.1038/364218a0
David, N.C., 1985. Excavation of the Abri Pataud, Les Eyzies (Dordogne): The Noaillian (Level 4) Assemblage and the Noaillian Culture in Western Europe, Bulletin (American School of Prehistoric Research. Harvard University Press, Cambridge, Massachusetts.
Debout, G., Olive, M., Bignon, O., Bodu, P., Chehmana, L., Valentin, B., 2012. The Magdalenian in the Paris Basin: New results. Quat. Int., The Magdalenian Settlement of Europe 272–273, 176–190. https://doi.org/10.1016/j.quaint.2012.05.016
Delvigne, V., 2016. Géoressources et expressions technoculturelles dans le sud du Massif central au Paléolithique supérieur : des déterminismes et des choix (Unpublished Ph.D. dissertation). University of Bordeaux, Talence.
Discamps, E., Gravina, B., Teyssandier, N., 2015. In the eye of the beholder: contextual issues for Bayesian modelling at the Middle-to-Upper Palaeolithic transition. World Archaeol. 47, 601–621. https://doi.org/10.1080/00438243.2015.1065759
Ducasse, S., 2012. What is left of the Badegoulian "interlude"? New data on cultural evolution in southern France between 23,500 and 20,500 cal. BP. Quat. Int. 272–273, 150–165. https://doi.org/10.1016/j.quaint.2012.05.018
Ducasse, S., 2010. La "parenthèse" badegoulienne : fondements et statut d'une discordance industrielle au travers de l'analyse techno-économique de plusieurs ensembles lithiques médidionaux du Dernier Maximum Glaciaire (Unpublished Ph.D. dissertation). University of Toulouse 2 Le Mirail, Toulouse.
Ducasse, S., Castel, J.-C., Chauvière, F.-X., Langlais, M., Camus, H., Morala, A., Turq, A., 2011. Le Quercy au cœur du dernier maximum glaciaire. La couche 4 du Petit Cloup Barrat et la question de la transition badegoulo-magdalénienne. PALEO Rev. Archéologie Préhistorique 101–154.
Ducasse, S., Pétillon, J.-M., Chauvière, F.-X., Renard, C., Lacrampe-Cuyaubère, F., Muth, X., 2019. Archaeological recontextualization and first direct 14C dating of a "pseudo-excise" decorated antler point from France (Pégourié Cave, Lot). Implications on the cultural geography of southwestern Europe during the Last Glacial Maximum. J. Archaeol. Sci. Rep. 23, 592–616. https://doi.org/10.1016/j.jasrep.2018.11.019
Ducasse, S., Pétillon, J.-M., Renard, C., 2014a. Le cadre radiométrique de la séquence solutréo-badegoulienne du Cuzoul de Vers (Lot, France) : lecture critique et compléments. PALEO Rev. Archéologie Préhistorique 25, 37–58.
Ducasse, S., Renard, C., Baumann, M., Bourdier, C., Castel, J.-C., Chalard, P., Chauvière, F.-X., Peschaux, C., Pétillon, J.-M., 2014b. Questioning the Solutrean-Badegoulian transition. A multidisciplinary approach based on data from southwest France.
Ducasse, S., Renard, C., Pétillon, J.-M., Costamagno, S., Foucher, P., San Juan-Foucher, C., Caux, S., 2017. Les Pyrénées au cours du Dernier Maximum Glaciaire Un no man's land badegoulien? Nouvelles données sur l'occupation du piémont pyrénéen à partir du réexamen des industries solutréennes de l'abri des Harpons (Lespugue, Haute-Garonne). Bull. Société Préhistorique Fr. 114, 257–294.
Duprat-Oualid, F., Rius, D., Bégeot, C., Magny, M., Millet, L., Wulf, S., Appelt, O., 2017. Vegetation response to abrupt climate changes in Western Europe from 45 to 14.7k cal a BP: the Bergsee

lacustrine record (Black Forest, Germany). J. Quat. Sci. 32, 1008–1021. https://doi.org/10.1002/jqs.2972
Dye, T.S., 2016. Long-term rhythms in the development of Hawaiian social stratification. J. Archaeol. Sci. 71, 1–9. https://doi.org/10.1016/j.jas.2016.05.006
Dye, T.S., Buck, C.E., 2015. Archaeological sequence diagrams and Bayesian chronological models. J. Archaeol. Sci. 63, 84–93. https://doi.org/10.1016/j.jas.2015.08.008
Eichhorn, L., Pirrung, M., Zolitschka, B., Büchel, G., 2017. Pleniglacial sedimentation process reconstruction on laminated lacustrine sediments from lava-dammed Paleolake Alf, West Eifel Volcanic Field (Germany). Quat. Sci. Rev. 172, 83–95. https://doi.org/10.1016/j.quascirev.2017.07.009
Elliot, M., Labeyrie, L., Dokken, T., Manthé, S., 2001. Coherent patterns of ice-rafted debris deposits in the Nordic regions during the last glacial (10–60 ka). Earth Planet. Sci. Lett. 194, 151–163. https://doi.org/10.1016/S0012-821X(01)00561-1
Fagnart, J.-P., Coudret, P., ANTOINE, P., Vallin, L., Sellier, N., Masson, B., 2013. Le Paléolithique supérieur ancien dans le Nord de la France, in: Bodu, P., Chehmana, L., Klaric, L., Mevel, L., Soriano, S., Teyssandier, N. (Eds.), Le Paléolithique Supérieur Ancien de l'Europe Du Nord-Ouest. Réflexions et Synthèses à Partir d'un Projet Collectif de Recherche Sur Le Centre et Le Sud Du Bassin Parisien, Mémoire de La SPF. Société préhistorique française, Paris, pp. 197–214.
Fletcher, W.J., Sánchez Goñi, M.F., Allen, J.R.M., Cheddadi, R., Combourieu-Nebout, N., Huntley, B., Lawson, I., Londeix, L., Magri, D., Margari, V., Müller, U.C., Naughton, F., Novenko, E., Roucoux, K., Tzedakis, P.C., 2010. Millennial-scale variability during the last glacial in vegetation records from Europe. Quat. Sci. Rev. 29, 2839–2864. https://doi.org/10.1016/j.quascirev.2009.11.015
Foucher, P., San Juan, C., Martin, H., 2000. Le site gravettien de la Carane-3 Foix, Ariège. Bull. Société Préhistorique Ariège-Pyrén. 54, 15–42.
Foucher, P., San Juan, C., Valladas, H., Clottes, J., Begouën, R., Giraud, J.-P., 2001. De nouvelles dates 14C pour le Gravettien des Pyrénées centrales. Bull. Société Préhistorique Ariège-Pyrén. 56, 35–44.
Foucher, P., San Juan-Foucher, C., Oberlin, C., 2011. Les niveaux d'occupation gravettiens de Gargas (Hautes-Pyrénées) : nouvelles données chronostratigraphiques, in: Goutas, N., Klaric, L., Pesesse, D., Guillermin, P. (Eds.), À La Recherche Des Identités Gravettiennes : Actualités, Questionnements, Perspectives, Mémoire. Société Préhistorique française, Paris, pp. 373–385.
Foucher, P., San Juan-Foucher, C., Sacchi, D., Arrizabalaga, Á., 2008. Le Gravettien des Pyrénées. PALEO Rev. Archéologie Préhistorique 331–356.
Gelfand, A.E., Hills, S.E., Racine-Poon, A., Smith, A.F.M., 1990. Illustration of Bayesian Inference in Normal Data Models Using Gibbs Sampling. J. Am. Stat. Assoc. 85, 972–985. https://doi.org/10.1080/01621459.1990.10474968
Geman, S., Geman, D., 1984. Stochastic Relaxation, Gibbs Distributions, and the Bayesian Restoration of Images. IEEE Trans. Pattern Anal. Mach. Intell. PAMI-6, 721–741. https://doi.org/10.1109/TPAMI.1984.4767596
Giaccio, B., Hajdas, I., Isaia, R., Deino, A., Nomade, S., 2017. High-precision ^{14}C and $^{40}Ar/^{39}Ar$ dating of the Campanian Ignimbrite (Y-5) reconciles the time-scales of climatic-cultural processes at 40 ka. Sci. Rep. 7, 45940. https://doi.org/10.1038/srep45940
Gowlett, J. a. J., Hedges, R.E.M., Law, I.A., Perry, C., 1987. Radiocarbon Dates from the Oxford Ams System: Archaeometry Datelist 5. Archaeometry 29, 125–155. https://doi.org/10.1111/j.1475-4754.1987.tb00404.x
Haesaerts, P., Damblon, F., Nigst, P., Hublin, J.-J., 2013. ABA and ABOx Radiocarbon Cross-Dating on Charcoal from Middle Pleniglacial Loess Deposits in Austria, Moravia, and Western Ukraine. Radiocarbon 55. https://doi.org/10.2458/azu_js_rc.55.16344

Hemming, S.R., 2004. Heinrich events: Massive late Pleistocene detritus layers of the North Atlantic and their global climate imprint. Rev. Geophys. 42. https://doi.org/10.1029/2003RG000128
Higham, T., 2011. European Middle and Upper Palaeolithic radiocarbon dates are often older than they look: problems with previous dates and some remedies. Antiquity 85, 235–249.
Higham, T., Douka, K., Wood, R., Ramsey, C.B., Brock, F., Basell, L., Camps, M., Arrizabalaga, A., Baena, J., Barroso-Ruíz, C., Bergman, C., Boitard, C., Boscato, P., Caparrós, M., Conard, N.J., Draily, C., Froment, A., Galván, B., Gambassini, P., Garcia-Moreno, A., Grimaldi, S., Haesaerts, P., Holt, B., Iriarte-Chiapusso, M.-J., Jelinek, A., Jordá Pardo, J.F., Maíllo-Fernández, J.-M., Marom, A., Maroto, J., Menéndez, M., Metz, L., Morin, E., Moroni, A., Negrino, F., Panagopoulou, E., Peresani, M., Pirson, S., de la Rasilla, M., Riel-Salvatore, J., Ronchitelli, A., Santamaria, D., Semal, P., Slimak, L., Soler, J., Soler, N., Villaluenga, A., Pinhasi, R., Jacobi, R., 2014. The timing and spatiotemporal patterning of Neanderthal disappearance. Nature 512, 306–309. https://doi.org/10.1038/nature13621
Higham, T., Jacobi, R., Basell, L., Ramsey, C.B., Chiotti, L., Nespoulet, R., 2011. Precision dating of the Palaeolithic: A new radiocarbon chronology for the Abri Pataud (France), a key Aurignacian sequence. J. Hum. Evol. 61, 549–563. https://doi.org/10.1016/j.jhevol.2011.06.005
Higham, T., Jacobi, R., Julien, M., David, F., Basell, L., Wood, R., Davies, W., Ramsey, C.B., 2010. Chronology of the Grotte du Renne (France) and implications for the context of ornaments and human remains within the Châtelperronian. Proc. Natl. Acad. Sci. 107, 20234–20239. https://doi.org/10.1073/pnas.1007963107
Higham, T.G., Jacobi, R.M., Ramsey, C.B., 2006. AMS Radiocarbon Dating Of Ancient Bone Using Ultrafiltration. Radiocarbon 48, 179–195. https://doi.org/10.2458/azu_js_rc.48.2861
Hinguant, S., Colleter, R., 2010. Le Solutréen de la grotte Rochefort (Saint-Pierre-sur-Erve, Mayenne) (Excavation Report). SRA Pays de la Loire, Rennes.
Hughes, P.D., Gibbard, P.L., 2015. A stratigraphical basis for the Last Glacial Maximum (LGM). Quat. Int., The Quaternary System and its formal subdivision 383, 174–185. https://doi.org/10.1016/j.quaint.2014.06.006
Jones, M., Nicholls, G., 2002. New Radiocarbon Calibration Software. Radiocarbon 44, 663–674. https://doi.org/10.1017/S0033822200032112
Kasse, C., 2002. Sandy aeolian deposits and environments and their relation to climate during the Last Glacial Maximum and Lateglacial in northwest and central Europe. Prog. Phys. Geogr. 26, 507–532. https://doi.org/10.1191/0309133302pp350ra
Kelly, R.L., 2013. The Lifeways of Hunter-Gatherers: The Foraging Spectrum, Second. ed. Cambridge University Press, New York.
Klaric, L. (Ed.), 2018. The prehistoric apprentice: Investigating apprenticeship, know-how and expertise in prehistoric technologies., The Dolni Vestonice Studies. Czech Academy of Sciences, Institute of Archaeology, Brno.
Klaric, L., 2017. « La réussite d'une production repose sur l'attention prêtée aux détails »: l'exemple des débitages lamellaires par méthode du Raysse (Gravettien moyen, France). J. Lithic Stud. 4, 387–421. https://doi.org/10.2218/jls.v4i2.2547
Klaric, L., 2013. Faciès lithiques et chronologie du Gravettien du sud du Bassin parisien et de sa marge sud-occidentale, in: Bodu, P., Chehmana, L., Klaric, L., Mevel, L., Soriano, S., Teyssandier, N. (Eds.), Le Paléolithique Supérieur Ancien de l'Europe Du Nord-Ouest. Réflexions et Synthèses à Partir d'un Projet Collectif de Recherche Sur Le Centre et Le Sud Du Bassin Parisien, Memoire de La SPF. Société Préhistorique Française, Paris, pp. 61–87.
Klaric, L., 2008. Anciennes et nouvelles hypothèses d'interprétation du gravettien moyen en France : la question de la place des industries à burins du Raysse au sein de la mosaïque gravettienne. PALEO Rev. Archéologie Préhistorique 257–276.

Klaric, L., 2007. Regional groups in the European Middle Gravettian: a reconsideration of the Rayssian technology. Antiquity 81, 176–190. https://doi.org/10.1017/S0003598X00094928
Klaric, L., 2003. L'unité technique des industries à burins du Raysse dans leur contexte diachronique. Réflexions sur la variabilité culturelle au Gravettien à partir des exemples de la Picardie, d'Arcy-sur-Cure, de Brassempouy et du Cirque de la Patrie. (Unpublished Ph.D. dissertation). Université Panthéon-Sorbonne - Paris I.
Lafarge, A., 2014. Entre plaine et montagne: Techniques et cultures du Badegoulien du Massif central, de l'Allier au Velay (Unpublished Ph.D. dissertation). University of Montpellier III, Montpellier.
Lane, C.S., Blockley, S.P.E., Lotter, A.F., Finsinger, W., Filippi, M.L., Matthews, I.P., 2012. A regional tephrostratigraphic framework for central and southern European climate archives during the Last Glacial to Interglacial transition: comparisons north and south of the Alps. Quat. Sci. Rev., The INTegration of Ice core, Marine and TErrestrial records of the last termination (INTIMATE) 60,000 to 8000 BP 36, 50–58. https://doi.org/10.1016/j.quascirev.2010.10.015
Lane, C.S., Brauer, A., Blockley, S.P.E., Dulski, P., 2013. Volcanic ash reveals time-transgressive abrupt climate change during the Younger Dryas. Geology 41, 1251–1254. https://doi.org/10.1130/G34867.1
Langlais, M., Ladier, E., Chalard, P., Jarry, M., Lacrampe-Cuyaubère, F., 2007. Aux origines du Magdalénien « classique » : les industries de la séquence inférieure de l'Abri Gandil (Bruniquel, Tarn-et-Garonne). PALEO Rev. Archéologie Préhistorique 341–366.
Lanos, P., Dufresne, P., 2019a. Chronomodel version 2.0: Software for Chronological Modelling of Archaeological Data using Bayesian Statistics. Centre National de la Recherche Scientifique.
Lanos, P., Dufresne, P., 2019b. ChronoModel version 2.0: User manual.
Lanos, P., Dufresne, P., 2012. Modélisation statistique bayésienne des données chronologiques, in: Beaune, S.A., Francfort, H.-P. (Eds.), L'Archéologie à Découvert. Paris, pp. 238–248.
Lanos, P., Philippe, A., 2018. Event date model: a robust Bayesian tool for chronology building. Commun. Stat. Appl. Methods 25, 131–157. https://doi.org/10.29220/CSAM.2018.25.2.131
Lanos, P., Philippe, A., 2017. Hierarchical Bayesian modeling for combining dates in archeological context. J. Société Fr. Stat. 158, 72–88.
Laville, H., Rigaud, J.-P., 1973. The Perigordian V industries in Périgord : typological variation, stratigraphy, relative chronology. World Archaeol. 4, 330–338.
Lelouvier, L.-A., 1996. Le Magdalénien initial du gisement du Cuzoul (Vers, Lot.). Approche techno-économique de l'industrie lithique de la couche 23 (Unpublished Master's thesis). University of Paris X, Nanterre.
Lenoble, A., Cosgrove, R., 2012. Les Eyzies-de-Tayac-Sireuil, Laugerie-Haute Ouest. Bilan Sci. Régional Aquitaine, 41–42.
Lenoir, M., Marmier, F., Trécolle, G., 1994. Le gisement magdalénien de Saint-Germain-la-Rivière (Gironde) : données anciennes et acquis récents. Rev. Archéologique Bordx. 85, 39–72.
Litton, C.D., Buck, C.E., 1995. The Bayesian Approach to the Interpretation of Archaeological Data. Archaeometry 37, 1–24. https://doi.org/10.1111/j.1475-4754.1995.tb00723.x
Lynch-Stieglitz, J., Schmidt, M.W., Gene Henry, L., Curry, W.B., Skinner, L.C., Mulitza, S., Zhang, R., Chang, P., 2014. Muted change in Atlantic overturning circulation over some glacial-aged Heinrich events. Nat. Geosci. 7, 144–150. https://doi.org/10.1038/ngeo2045
Marom, A., McCullagh, J.S.O., Higham, T.F.G., Hedges, R.E.M., 2013. Hydroxyproline Dating: Experiments on the 14C Analysis of Contaminated and Low-Collagen Bones. Radiocarbon 55. https://doi.org/10.2458/azu_js_rc.55.16301
Marom, A., McCullagh, J.S.O., Higham, T.F.G., Sinitsyn, A.A., Hedges, R.E.M., 2012. Single amino acid radiocarbon dating of Upper Paleolithic modern humans. Proc. Natl. Acad. Sci. 109, 6878–6881. https://doi.org/10.1073/pnas.1116328109

McManus, J.F., Francois, R., Gherardi, J.-M., Keigwin, L.D., Brown-Leger, S., 2004. Collapse and rapid resumption of Atlantic meridional circulation linked to deglacial climate changes. Nature 428, 834–837. https://doi.org/10.1038/nature02494
Mellars, P.A., Bricker, H.M., Gowlett, J.A.J., Hedges, R.E.M., 1987. Radiocarbon Accelerator Dating of French Upper Palaeolithic Sites. Curr. Anthropol. 28, 128–133.
Montet-White, A., Evin, J., Stafford, T., 2002. Les datations radiocarbone des amas osseux de Solutré, in: Combier, J., Montet-White, A. (Eds.), Solutré : 1968-1998, Mémoire de La SPF. Société préhistorique française, Paris, pp. 181–189.
Movius, H.L., Jr. (Ed.), 1975. Excavation of the Abri Pataud, Les Eyzies (Dordogne), American School of Prehistoric Research. Peabody Museum, Harvard University, Cambridge, Massachusetts.
Muscheler, R., Adolphi, F., Svensson, A., 2014. Challenges in 14C dating towards the limit of the method inferred from anchoring a floating tree ring radiocarbon chronology to ice core records around the Laschamp geomagnetic field minimum. Earth Planet. Sci. Lett. 394, 209–215. https://doi.org/10.1016/j.epsl.2014.03.024
Naughton, F., Sánchez Goñi, M.F., Kageyama, M., Bard, E., Duprat, J., Cortijo, E., Desprat, S., Malaizé, B., Joly, C., Rostek, F., Turon, J.-L., 2009. Wet to dry climatic trend in north-western Iberia within Heinrich events. Earth Planet. Sci. Lett. 284, 329–342. https://doi.org/10.1016/j.epsl.2009.05.001
Naylor, J.C., Smith, A.F.M., 1988. An Archaeological Inference Problem. J. Am. Stat. Assoc. 83, 588–595. https://doi.org/10.1080/01621459.1988.10478638
Nespoulet, R., Chiotti, L., Henry-Gambier, D., 2013. Le Gravettien final de l'abri Pataud (Dordogne, France), BAR International Series. Archaeopress, Oxford.
Oberlin, C., Valladas, H., 2012. Le Cadre Chronologique: Datation 14C, in: Clottes, J., Giraud, J.-P., Chalard, P. (Eds.), Solutréen et Badegoulien Au Cuzoul de Vers : Des Chasseurs de Rennes En Quercy, ERAUL. Liège, pp. 79–84.
Paris, C., Deneuve, E., Fagnart, J.-P., Coudret, P., Antoine, P., Peschaux, C., Lacarriere, J., Coutard, S., Moine, O., Guérin, G., 2017. Premières observations sur le gisement gravettien à statuettes féminines d'Amiens-Renancourt 1 (Somme). Bull. Société Préhistorique Fr. 114, 423–444.
Paris, C., Fagnart, J.-P., Coudret, P., 2013. Du Gravettien final dans le Nord de la France ? Nouvelles données à Amiens-Renancourt (Somme, France). Bull. Société Préhistorique Fr. 110, 123–126. https://doi.org/10.3406/bspf.2013.14234
Parker, A.O., Schmidt, M.W., Chang, P., 2015. Tropical North Atlantic subsurface warming events as a fingerprint for AMOC variability during Marine Isotope Stage 3. Paleoceanography 30, 1425–1436. https://doi.org/10.1002/2015PA002832
Pétillon, J.-M., Ducasse, S., 2012. From flakes to grooves: A technical shift in antlerworking during the last glacial maximum in southwest France. J. Hum. Evol. 62, 435–465. https://doi.org/10.1016/j.jhevol.2011.12.005
Pettitt, P., Zilhão, J., 2015. Problematizing Bayesian approaches to prehistoric chronologies. World Archaeol. 47, 525–542. https://doi.org/10.1080/00438243.2015.1070082
Pottier, C., 2005. Le Gravettien moyen de l'abri Pataud (Dordogne, France): le niveau 4 et l'éboulis 3/4. Etude typologique et technologique de l'industrie lithique (Unpublished Ph.D. dissertation). Muséum National d'Histoire Naturelle, Paris.
Primault, J., Berthet, A.-L., Brou, L., Delfour, G., Gabilleau, J., Griggo, C., Guérin, S., Henry-Gambier, D., Houmard, C., Jeannet, M., Lacrampe-Cuyaubère, F., Langlais, M., Laroulandie, V., Liard, M., Liolios, D., Lompre, A., Lucquin, A., Mistrot, V., Rambaud, D., Schmitt, A., Soler, L., Taborin, Y., Vissac, C., 2010. La grotte du Taillis des Coteaux à Antigny (Vienne), in: Buisson-Catil, J., Primault, J. (Eds.), Préhistoire entre Vienne et Charente: Hommes et Sociétés du Paléolithique, Memoire. Association des Publications Chauvinoises, Chauvigny, pp. 271–293.

Rasmussen, S.O., Bigler, M., Blockley, S.P., Blunier, T., Buchardt, S.L., Clausen, H.B., Cvijanovic, I., Dahl-Jensen, D., Johnsen, S.J., Fischer, H., Gkinis, V., Guillevic, M., Hoek, W.Z., Lowe, J.J., Pedro, J.B., Popp, T., Seierstad, I.K., Steffensen, J.P., Svensson, A.M., Vallelonga, P., Vinther, B.M., Walker, M.J.C., Wheatley, J.J., Winstrup, M., 2014. A stratigraphic framework for abrupt climatic changes during the Last Glacial period based on three synchronized Greenland ice-core records: refining and extending the INTIMATE event stratigraphy. Quat. Sci. Rev. 106, 14–28. https://doi.org/10.1016/j.quascirev.2014.09.007

Raynal, J.-P., Lafarge, A., Rémy, D., Delvigne, V., Guadelli, J.-L., Costamagno, S., Le Gall, O., Daujeard, C., Vivent, D., Fernandes, P., Le Corre-le Beux, M., Vernet, G., Bazile, F., Lefèvre, D., 2014a. Datations SMA et nouveaux regards sur l'archéo-séquence du Rond-du-Barry (Polignac, Haute-Loire). Comptes Rendus Palevol 13, 623–636. https://doi.org/10.1016/j.crpv.2014.03.010

Raynal, J.-P., Lafarge, A., Rémy, D., Delvigne, V., Guadelli, J.-L., Costamagno, S., Le Gall, O., Daujeard, C., Vivent, D., Fernandes, P., Le Corre-le Beux, M., Vernet, G., Bazile, F., Lefèvre, D., 2014b. Datations SMA et nouveaux regards sur l'archéo-séquence du Rond-du-Barry (Polignac, Haute-Loire). Comptes Rendus Palevol 13, 623–636. https://doi.org/10.1016/j.crpv.2014.03.010

Reimer, P.J., Baillie, M.G.L., Bard, E., Bayliss, A., Beck, J.W., Blackwell, P.G., Ramsey, C.B., Buck, C.E., Burr, G.S., Edwards, R.L., Friedrich, M., Grootes, P.M., Guilderson, T.P., Hajdas, I., Heaton, T.J., Hogg, A.G., Hughen, K.A., Kaiser, K.F., Kromer, B., McCormac, F.G., Manning, S.W., Reimer, R.W., Richards, D.A., Southon, J.R., Talamo, S., Turney, C.S.M., Plicht, J. van der, Weyhenmeyer, C.E., 2009. IntCal09 and Marine09 Radiocarbon Age Calibration Curves, 0-50,000 Years cal BP. Radiocarbon 51, 1111–1150. https://doi.org/10.2458/rc.v51i4.3569

Reimer, P.J., Bard, E., Bayliss, A., Beck, J.W., Blackwell, P.G., Bronk Ramsey, C., Buck, C.E., Cheng, H., Edwards, R.L., Friedrich, M., Grootes, P.M., Guilderson, T.P., Haflidason, H., Hajdas, I., Hatte, C., Heaton, T.J., Hoffmann, D.L., Hogg, A.G., Hughen, K.A., Kaiser, K.F., Kromer, B., Manning, S.W., Niu, M., Reimer, R.W., Richards, D.A., Scott, E.M., Southon, J.R., Staff, R.A., Turney, C.S.M., van der Plicht, J., 2013. IntCal13 and Marine13 Radiocarbon Age Calibration Curves 0–50,000 Years cal BP. Radiocarbon 55, 1869–1887. https://doi.org/10.2458/azu_js_rc.55.16947

Renard, C., 2011. Continuity or discontinuity in the Late Glacial Maximum of south-western Europe: the formation of the Solutrean in France. World Archaeol. 43, 726–743. https://doi.org/10.1080/00438243.2011.624789

Renard, C., 2010. Les premières expressions du Solutréen dans le Sud-Ouest français : Evolution techno-économique des équipements lithiques au cours du Dernier Maximum Glaciaire, BAR International Series. John and Erica Hedges Ltd., Oxford.

Renard, C., Ducasse, S., 2015. De la rupture typologique à la fracture socio-économique. Implications sur les systèmes de mobilité entre Solutréen récent et Badegoulien dans le Sud-Ouest français (24-21 ka cal. BP), in: Naudinot, N., Meignen, L., Binder, D., Querré, G. (Eds.), Les Systèmes de Mobilité de La Préhistoire Au Moyen-Âge, Actes Des XXXVe Rencontres Internationales d'archéologie et d'histoire (Antibes, 14-16 Octobre 2014). APDCA, Antibes, pp. 193–208.

Rigaud, J.-P., 1988. The Gravettian Peopling of Southwestern France: Taxonomic Problems, in: Dibble, H.L., Montet-White, A. (Eds.), Upper Pleistocene Prehistory of Western Eurasia, University Museum Monographs. The University Museum, University of Pennsylvanai, Philadelphia, pp. 387–396.

Rigaud, J.-P., Simek, J., Delpech, F., Texier, J.-P., 2016. L'Aurignacien et le Gravettien du nord de l'Aquitaine : la contribution du Flageolet I (Bézenac, Dordogne, France). PALEO Rev. Archéologie Préhistorique 265–295.

Rivals, F., Uzunidis, A., Sanz, M., Daura, J., 2017. Faunal dietary response to the Heinrich Event 4 in southwestern Europe. Palaeogeogr. Palaeoclimatol. Palaeoecol. 473, 123–130. https://doi.org/10.1016/j.palaeo.2017.02.033

Roque, C., Guibert, P., Vartanian, E., Bechtel, F., Oberlin, C., Evin, J., Mercier, N., Valladas, H., Texier, J.-P., Rigaud, J.-P., Delpech, F., Cleyet-Merle, J.-J., Turq, A., 2001. Une expérience de croisement de datations TL/14C pour la séquence solutréenne de Laugerie-Haute, Dordogne, in: Barrandon, J.-N., Guibert, P., Michel, V. (Eds.), XXI Rencontres Internationales d'archeologie et d'histoire d'Antibes. Antibes, pp. 217–232.

Sanchez Goñi, M.F., Harrison, S.P., 2010. Millennial-scale climate variability and vegetation changes during the Last Glacial: Concepts and terminology. Quat. Sci. Rev., Vegetation Response to Millennial-scale Variability during the Last Glacial 29, 2823–2827. https://doi.org/10.1016/j.quascirev.2009.11.014

Sánchez Goñi, M.F., Landais, A., Fletcher, W.J., Naughton, F., Desprat, S., Duprat, J., 2008. Contrasting impacts of Dansgaard–Oeschger events over a western European latitudinal transect modulated by orbital parameters. Quat. Sci. Rev. 27, 1136–1151. https://doi.org/10.1016/j.quascirev.2008.03.003

Sanchez Goñi, M.-F., Turon, J.-L., Eynaud, F., Gendreau, S., 2000. European Climatic Response to Millennial-Scale Changes in the Atmosphere–Ocean System during the Last Glacial Period. Quat. Res. 54, 394–403. https://doi.org/10.1006/qres.2000.2176

Sapin, C., Baylé, M., Büttner, S., Guibert, P., Blain, S., Lanos, P., Chauvin, A., Dufresne, P., Oberlin, C., 2008. Archéologie du bâti et archéométrie au Mont-Saint-Michel, nouvelles approches de Notre-Dame-sous-Terre. Archéologie Médiév. 38, 71–122.

Sommer, R.S., Nadachowski, A., 2006. Glacial refugia of mammals in Europe: evidence from fossil records. Mammal Rev. 36, 251–265. https://doi.org/10.1111/j.1365-2907.2006.00093.x

Surmely, F., Hays, M., 2011. Nouvelles données sur les industries lithiques des niveaux protomagdaléniens du site du Blot (Cerzat, Haute-Loire), in: Goutas, N., Klaric, L., Pesesse, D., Guillermin, P. (Eds.), À La Recherche Des Identités Gravettiennes : Actualités, Questionnements, Perspectives, Memoire de La SPF. Société Préhistorique française, Paris, pp. 111–127.

Teyssandier, N., Zilhão, J., 2018. On the Entity and Antiquity of the Aurignacian at Willendorf (Austria): Implications for Modern Human Emergence in Europe. J. Paleolit. Archaeol. 1–32. https://doi.org/10.1007/s41982-017-0004-4

Thompson, W.G., Goldstein, S.L., 2006. A radiometric calibration of the SPECMAP timescale. Quat. Sci. Rev., Critical Quaternary Stratigraphy 25, 3207–3215. https://doi.org/10.1016/j.quascirev.2006.02.007

Tisnerat-Laborde, N., Valladas, H., Ladier, E., 1997. Nouvelles datations carbone 14 en SMA pour le Magdalénien supérieur de la vallée de l'Aveyron. Bull. Société Préhistoire Ariège-Pyrén. 2, 129–136.

Touzé, O., 2013. De la signification du Noaillien et du Rayssien, in: de las Heras, C., Lasheras, J.A., Arrizabalaga, Á., de la Rasilla, M. (Eds.), Pensando El Gravetiense: Nuevos Datos Para La Región Cantábrica En Su Contexto Peninsular y Pirenaico, Monografías Del Museo Nacional y Centro de Investigación de Altamira. Museo Nacional y Centro de Investigación de Altamira, Madrid, pp. 383–400.

Turney, C.S.M., Palmer, J., Bronk Ramsey, C., Adolphi, F., Muscheler, R., Hughen, K.A., Staff, R.A., Jones, R.T., Thomas, Z.A., Fogwill, C.J., Hogg, A., 2016. High-precision dating and correlation of ice, marine and terrestrial sequences spanning Heinrich Event 3: Testing mechanisms of interhemispheric change using New Zealand ancient kauri (Agathis australis). Quat. Sci. Rev. 137, 126–134. https://doi.org/10.1016/j.quascirev.2016.02.005

Vandenberghe, J., French, H.M., Gorbunov, A., Marchenko, S., Velichko, A.A., Jin, H., Cui, Z., Zhang, T., Wan, X., 2014. The Last Permafrost Maximum (LPM) map of the Northern Hemisphere: permafrost extent and mean annual air temperatures, 25–17 ka BP. Boreas 43, 652–666. https://doi.org/10.1111/bor.12070

Vermeersch, P.M., 2005. European population changes during Marine Isotope Stages 2 and 3. Quat. Int., Armageddon or entente? The demise of the European Neandertals in Isotope Stage 3 137, 77–85. https://doi.org/10.1016/j.quaint.2004.11.021

Verpoorte, A., Cosgrove, R., Wood, R., Petchey, F., Lenoble, A., Chadelle, J.-P., Smith, C., Kamermans, H., Roebroeks, W., 2019. Improving the chronological framework for Laugerie-Haute Ouest (Dordogne, France). J. Archaeol. Sci. Rep. 23, 574–582. https://doi.org/10.1016/j.jasrep.2018.11.017

Vibet, M.-A., Philippe, A., Lanos, P., 2016. ChronoModel v1.5 user's manual.

Vignoles, A., 2018. Le Gravettien moyen en France: Exploration de liens potentiels entre variabilité technologique et écologique (Unpublishes Master's thesis). University of Bordeaux, Talence.

Whallon, R., 2006. Social networks and information: Non-"utilitarian" mobility among hunter-gatherers. J. Anthropol. Archaeol. 25, 259–270. https://doi.org/10.1016/j.jaa.2005.11.004

Zilhão, J., 2013. Seeing the leaves and not missing the forest: a Portuguese perspective of the Solutrean, in: Pastoors, A., Auffermann, B. (Eds.), Pleistocene Foragers on the Iberian Peninsula: Their Culture and Environment, Wisssenschaftliche Schriften Des Neanderthal Museums. Neanderthal Museum, Mettmann.

Zilhao, J., 2013. Forty Years after Roche 1964: A Far-West View of the Solutrean, in: Le Solutréen… 40 Ans Après Smith '66. ARCHEA/FERACF, Tours, pp. 87–99.

Zilhão, J., Banks, W.E., d'Errico, F., Gioia, P., 2015. Analysis of Site Formation and Assemblage Integrity Does Not Support Attribution of the Uluzzian to Modern Humans at Grotta del Cavallo. PLOS ONE 10, e0131181. https://doi.org/10.1371/journal.pone.0131181

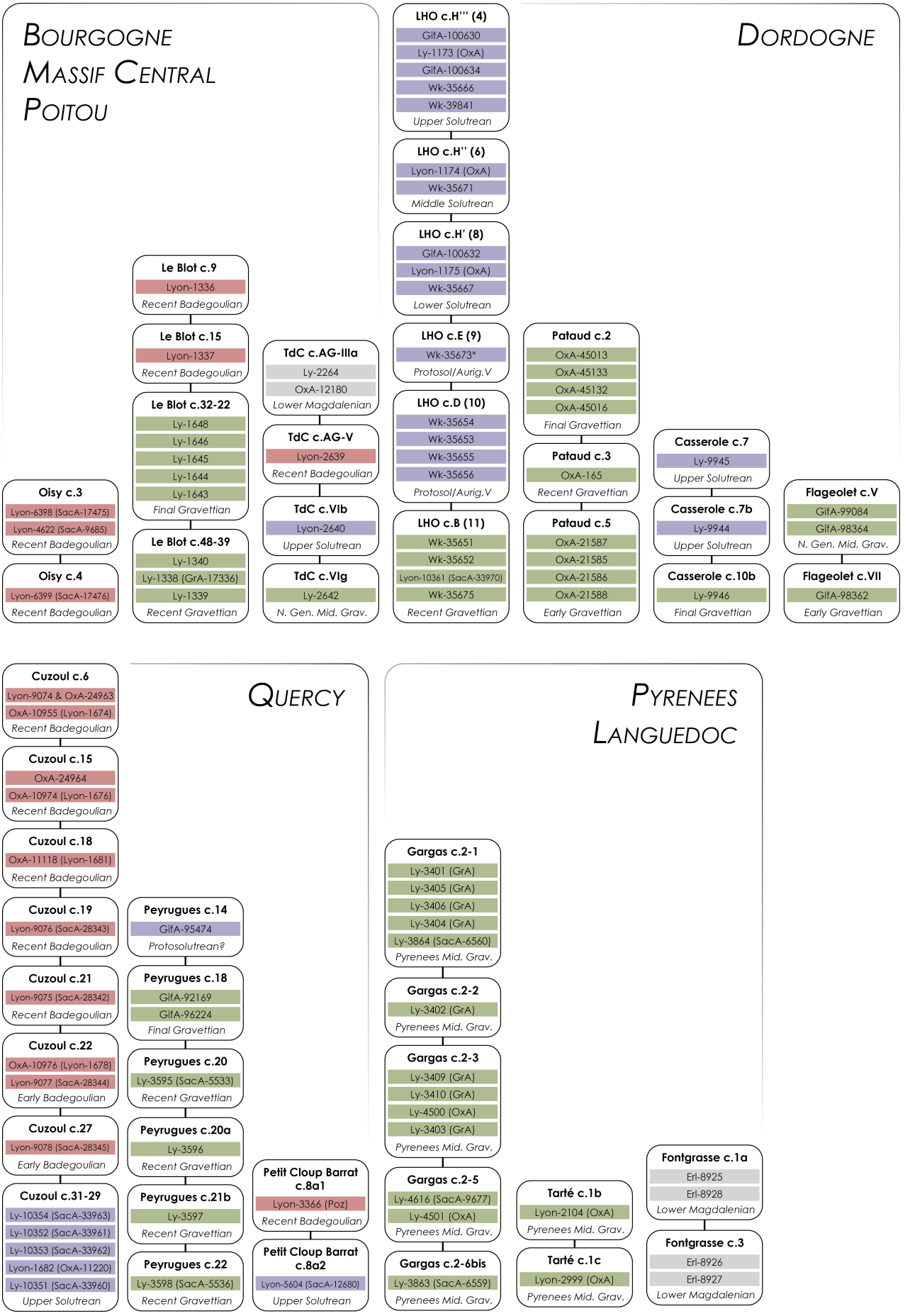
Bourgogne
Massif Central
Poitou
Dordogne
Quercy
Pyrenees
Languedoc
Oisy c.3
Lyon-6398 (SacA-17475)
Lyon-4622 (SacA-9685)
Recent Badegoulian
Oisy c.4
Lyon-6399 (SacA-17476)
Recent Badegoulian
Le Blot c.9
Lyon-1336
Recent Badegoulian
Le Blot c.15
Lyon-1337
Recent Badegoulian
Le Blot c.32-22
Ly-1648
Ly-1646
Ly-1645
Ly-1644
Ly-1643
Final Gravettian
Le Blot c.48-39
Ly-1340
Ly-1338 (GrA-17336)
Ly-1339
Recent Gravettian
TdC c.AG-IIIa
Ly-2264
OxA-12180
Lower Magdalenian
TdC c.AG-V
Lyon-2639
Recent Badegoulian
TdC c.VIb
Lyon-2640
Upper Solutrean
TdC c.VIg
Ly-2642
N. Gen. Mid. Grav.
LHO c.H''' (4)
GifA-100630
Ly-1173 (OxA)
GifA-100634
Wk-35666
Wk-39841
Upper Solutrean
LHO c.H'' (6)
Lyon-1174 (OxA)
Wk-35671
Middle Solutrean
LHO c.H' (8)
GifA-100632
Lyon-1175 (OxA)
Wk-35667
Lower Solutrean
LHO c.E (9)
Wk-35673*
Protosol/Aurig.V
LHO c.D (10)
Wk-35654
Wk-35653
Wk-35655
Wk-35656
Protosol/Aurig.V
LHO c.B (11)
Wk-35651
Wk-35652
Lyon-10361 (SacA-33970)
Wk-35675
Recent Gravettian
Pataud c.2
OxA-45013
OxA-45133
OxA-45132
OxA-45016
Final Gravettian
Pataud c.3
OxA-165
Recent Gravettian
Pataud c.5
OxA-21587
OxA-21585
OxA-21586
OxA-21588
Early Gravettian
Casserole c.7
Ly-9945
Upper Solutrean
Casserole c.7b
Ly-9944
Upper Solutrean
Casserole c.10b
Ly-9946
Final Gravettian
Flageolet c.V
GifA-99084
GifA-98364
N. Gen. Mid. Grav.
Flageolet c.VII
GifA-98362
Early Gravettian
Cuzoul c.6
Lyon-9074 & OxA-24963
OxA-10955 (Lyon-1674)
Recent Badegoulian
Cuzoul c.15
OxA-24964
OxA-10974 (Lyon-1676)
Recent Badegoulian
Cuzoul c.18
OxA-11118 (Lyon-1681)
Recent Badegoulian
Cuzoul c.19
Lyon-9076 (SacA-28343)
Recent Badegoulian
Cuzoul c.21
Lyon-9075 (SacA-28342)
Recent Badegoulian
Cuzoul c.22
OxA-10976 (Lyon-1678)
Lyon-9077 (SacA-28344)
Early Badegoulian
Cuzoul c.27
Lyon-9078 (SacA-28345)
Early Badegoulian
Cuzoul c.31-29
Ly-10354 (SacA-33963)
Ly-10352 (SacA-33961)
Ly-10353 (SacA-33962)
Lyon-1682 (OxA-11220)
Ly-10351 (SacA-33960)
Upper Solutrean
Peyrugues c.14
GifA-95474
Protosolutrean?
Peyrugues c.18
GifA-92169
GifA-96224
Final Gravettian
Peyrugues c.20
Ly-3595 (SacA-5533)
Recent Gravettian
Peyrugues c.20a
Ly-3596
Recent Gravettian
Peyrugues c.21b
Ly-3597
Recent Gravettian
Peyrugues c.22
Ly-3598 (SacA-5536)
Recent Gravettian
Petit Cloup Barrat c.8a1
Lyon-3366 (Poz)
Recent Badegoulian
Petit Cloup Barrat c.8a2
Lyon-5604 (SacA-12680)
Upper Solutrean
Gargas c.2-1
Ly-3401 (GrA)
Ly-3405 (GrA)
Ly-3406 (GrA)
Ly-3404 (GrA)
Ly-3864 (SacA-6560)
Pyrenees Mid. Grav.
Gargas c.2-2
Ly-3402 (GrA)
Pyrenees Mid. Grav.
Gargas c.2-3
Ly-3409 (GrA)
Ly-3410 (GrA)
Ly-4500 (OxA)
Ly-3403 (GrA)
Pyrenees Mid. Grav.
Gargas c.2-5
Ly-4616 (SacA-9677)
Ly-4501 (OxA)
Pyrenees Mid. Grav.
Gargas c.2-6bis
Ly-3863 (SacA-6559)
Pyrenees Mid. Grav.
Tarté c.1b
Lyon-2104 (OxA)
Pyrenees Mid. Grav.
Tarté c.1c
Lyon-2999 (OxA)
Pyrenees Mid. Grav.
Fontgrasse c.1a
Erl-8925
Erl-8928
Lower Magdalenian
Fontgrasse c.3
Erl-8926
Erl-8927
Lower Magdalenian

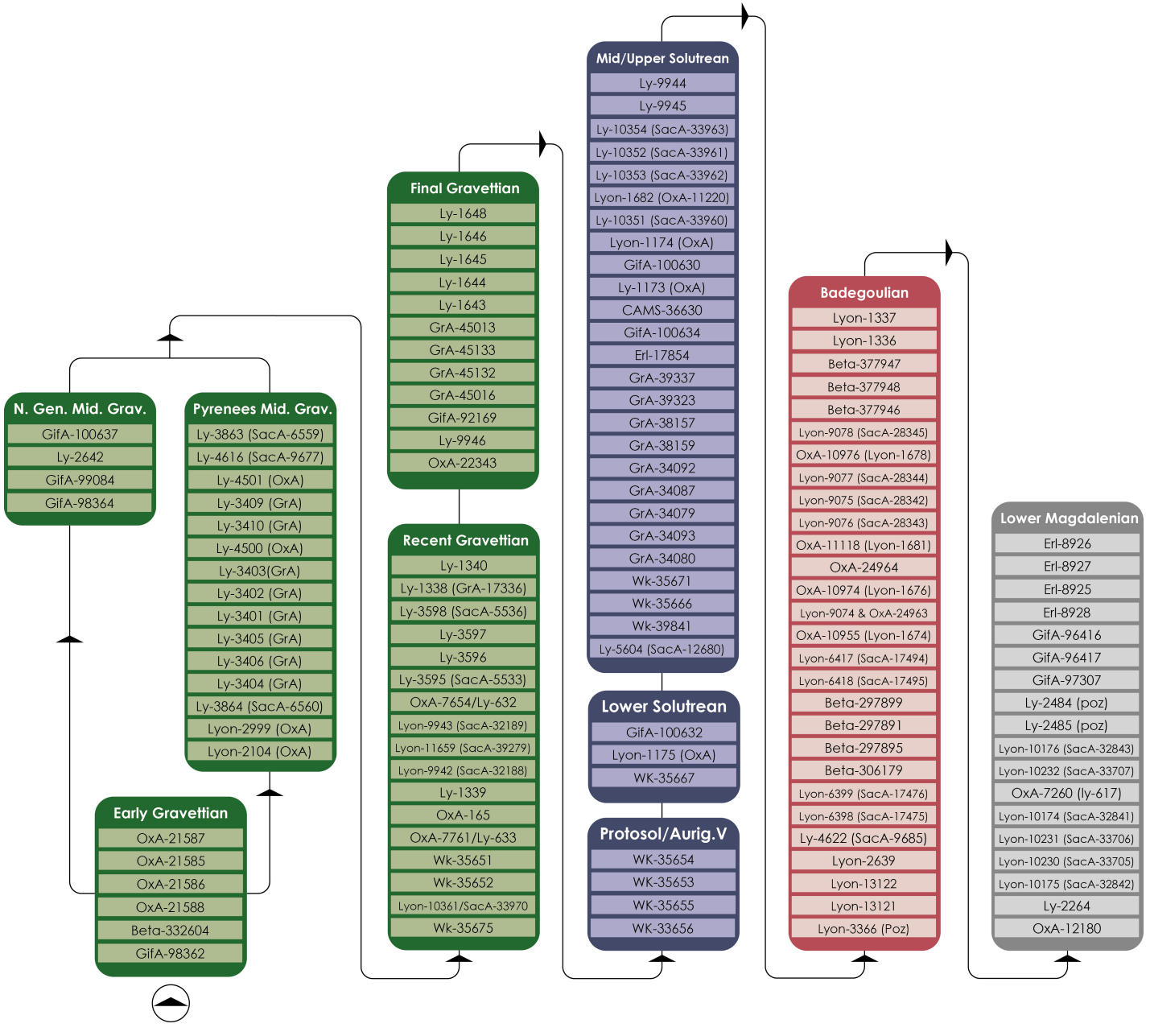
N. Gen. Mid. Grav.
GifA-100637
Ly-2642
GifA-99084
GifA-98364
Pyrenees Mid. Grav.
Ly-3863 (SacA-6559)
Ly-4616 (SacA-9677)
Ly-4501 (OxA)
Ly-3409 (GrA)
Ly-3410 (GrA)
Ly-4500 (OxA)
Ly-3403(GrA)
Ly-3402 (GrA)
Ly-3401 (GrA)
Ly-3405 (GrA)
Ly-3406 (GrA)
Ly-3404 (GrA)
Ly-3864 (SacA-6560)
Lyon-2999 (OxA)
Lyon-2104 (OxA)
Early Gravettian
OxA-21587
OxA-21585
OxA-21586
OxA-21588
Beta-332604
GifA-98362
Final Gravettian
Ly-1648
Ly-1646
Ly-1645
Ly-1644
Ly-1643
GrA-45013
GrA-45133
GrA-45132
GrA-45016
GifA-92169
Ly-9946
OxA-22343
Recent Gravettian
Ly-1340
Ly-1338 (GrA-17336)
Ly-3598 (SacA-5536)
Ly-3597
Ly-3596
Ly-3595 (SacA-5533)
OxA-7654/Ly-632
Lyon-9943 (SacA-32189)
Lyon-11659 (SacA-39279)
Lyon-9942 (SacA-32188)
Ly-1339
OxA-165
OxA-7761/Ly-633
Wk-35651
Wk-35652
Lyon-10361/SacA-33970
Wk-35675
Mid/Upper Solutrean
Ly-9944
Ly-9945
Ly-10354 (SacA-33963)
Ly-10352 (SacA-33961)
Ly-10353 (SacA-33962)
Lyon-1682 (OxA-11220)
Ly-10351 (SacA-33960)
Lyon-1174 (OxA)
GifA-100630
Ly-1173 (OxA)
CAMS-36630
GifA-100634
Erl-17854
GrA-39337
GrA-39323
GrA-38157
GrA-38159
GrA-34092
GrA-34087
GrA-34079
GrA-34093
GrA-34080
Wk-35671
Wk-35666
Wk-39841
Ly-5604 (SacA-12680)
Lower Solutrean
GifA-100632
Lyon-1175 (OxA)
WK-35667
Protosol/Aurig.V
WK-35654
WK-35653
WK-35655
WK-33656
Badegoulian
Lyon-1337
Lyon-1336
Beta-377947
Beta-377948
Beta-377946
Lyon-9078 (SacA-28345)
OxA-10976 (Lyon-1678)
Lyon-9077 (SacA-28344)
Lyon-9075 (SacA-28342)
Lyon-9076 (SacA-28343)
OxA-11118 (Lyon-1681)
OxA-24964
OxA-10974 (Lyon-1676)
Lyon-9074 & OxA-24963
OxA-10955 (Lyon-1674)
Lyon-6417 (SacA-17494)
Lyon-6418 (SacA-17495)
Beta-297899
Beta-297891
Beta-297895
Beta-306179
Lyon-6399 (SacA-17476)
Lyon-6398 (SacA-17475)
Ly-4622 (SacA-9685)
Lyon-2639
Lyon-13122
Lyon-13121
Lyon-3366 (Poz)
Lower Magdalenian
Erl-8926
Erl-8927
Erl-8925
Erl-8928
GifA-96416
GifA-96417
GifA-97307
Ly-2484 (poz)
Ly-2485 (poz)
Lyon-10176 (SacA-32843)
Lyon-10232 (SacA-33707)
OxA-7260 (ly-617)
Lyon-10174 (SacA-32841)
Lyon-10231 (SacA-33706)
Lyon-10230 (SacA-33705)
Lyon-10175 (SacA-32842)
Ly-2264
OxA-12180

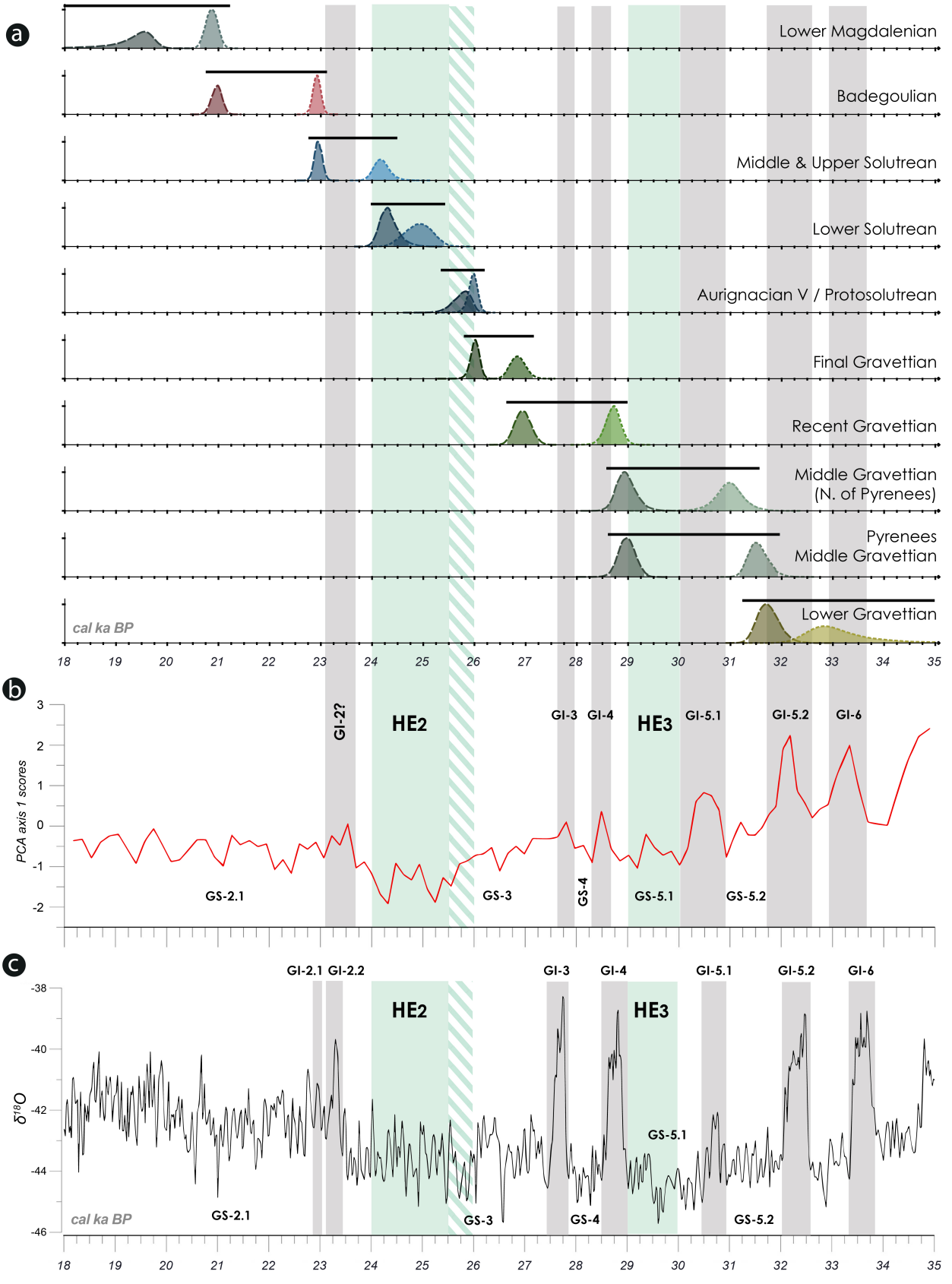
a
Lower Magdalenian
Badegoulian
Middle & Upper Solutrean
Lower Solutrean
Aurignacian V / Protosolutrean
Final Gravettian
Recent Gravettian
Middle Gravettian
(N. of Pyrenees)
Pyrenees
Middle Gravettian
Lower Gravettian
cal ka BP
18 19 20 21 22 23 24 25 26 27 28 29 30 31 32 33 34 35
b
PCA axis 1 scores
3 2 1 0 -1 -2
GI-2?
HE2
GI-3
GI-4
HE3
GI-5.1
GI-5.2
GI-6
GS-2.1
GS-3
GS-4
GS-5.1
GS-5.2
c
δ18O
-38 -40 -42 -44 -46
GI-2.1
GI-2.2
HE2
GI-3
GI-4
HE3
GI-5.1
GI-5.2
GI-6
GS-5.1
GS-2.1
GS-3
GS-4
GS-5.2
cal ka BP
18 19 20 21 22 23 24 25 26 27 28 29 30 31 32 33 34 35

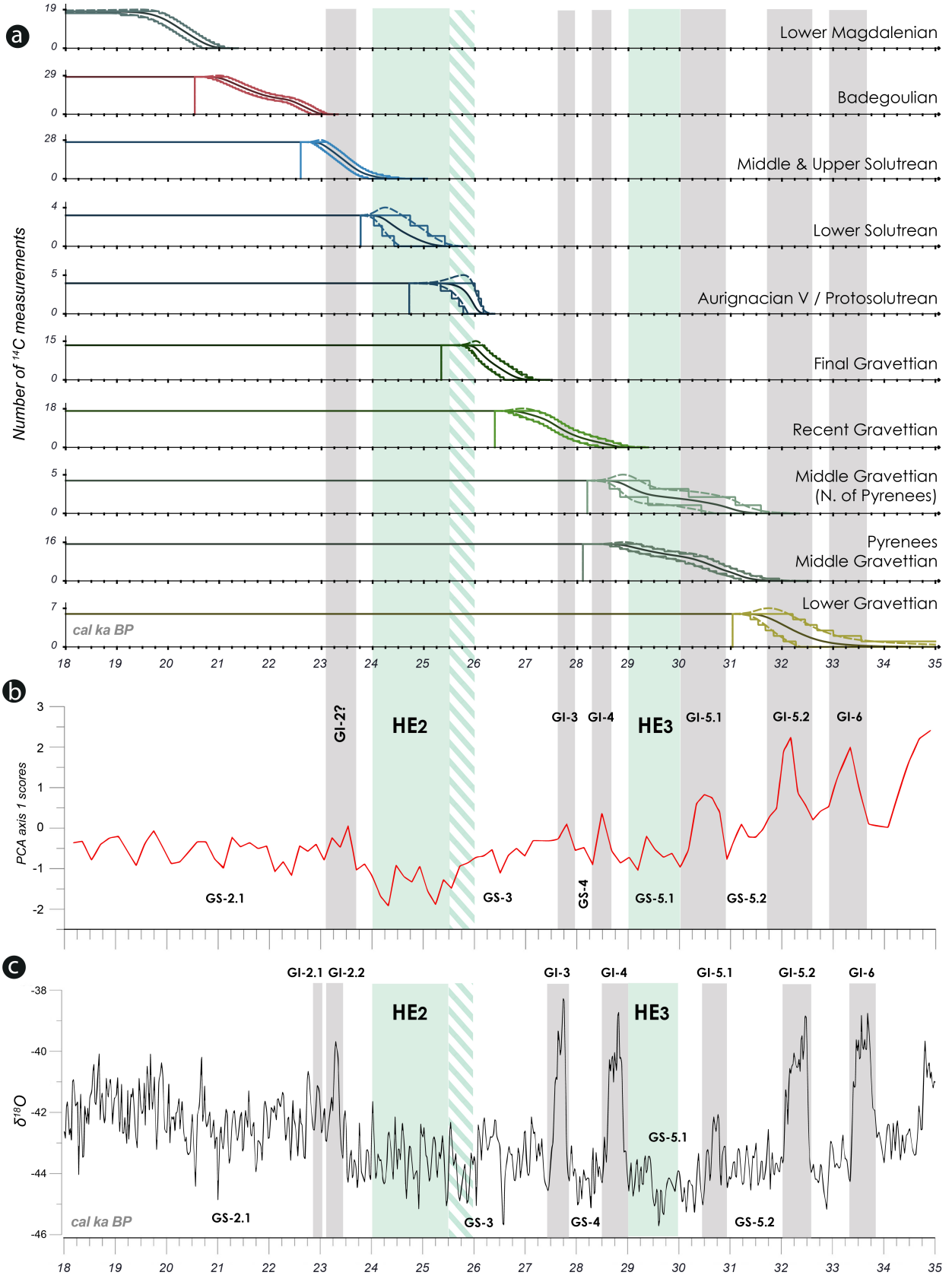
a
Number of ¹⁴C measurements
Lower Magdalenian
Badegoulian
Middle & Upper Solutrean
Lower Solutrean
Aurignacian V / Protosolutrean
Final Gravettian
Recent Gravettian
Middle Gravettian
(N. of Pyrenees)
Pyrenees
Middle Gravettian
Lower Gravettian
cal ka BP
b
PCA axis 1 scores
GI-2?
HE2
GI-3
GI-4
HE3
GI-5.1
GI-5.2
GI-6
GS-2.1
GS-3
GS-4
GS-5.1
GS-5.2
c
δ¹⁸O
GI-2.1
GI-2.2
HE2
GI-3
GI-4
HE3
GI-5.1
GI-5.2
GI-6
GS-2.1
GS-3
GS-4
GS-5.1
GS-5.2
cal ka BP

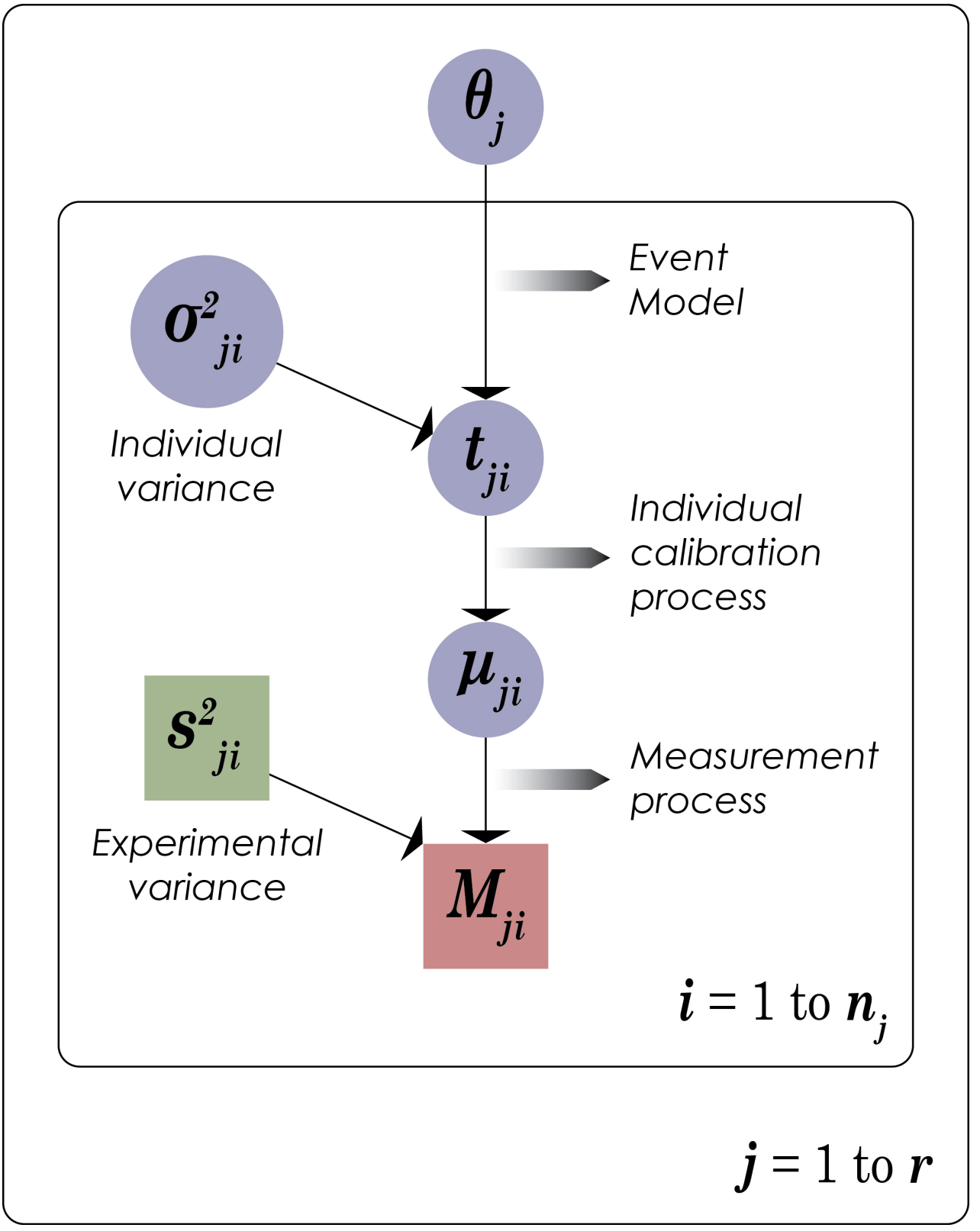
θ_j
Event Model
σ^2_{ji}
Individual variance
t_{ji}
Individual calibration process
μ_{ji}
s^2_{ji}
Measurement process
Experimental variance
M_{ji}
$i = 1$ to n_j
$j = 1$ to r

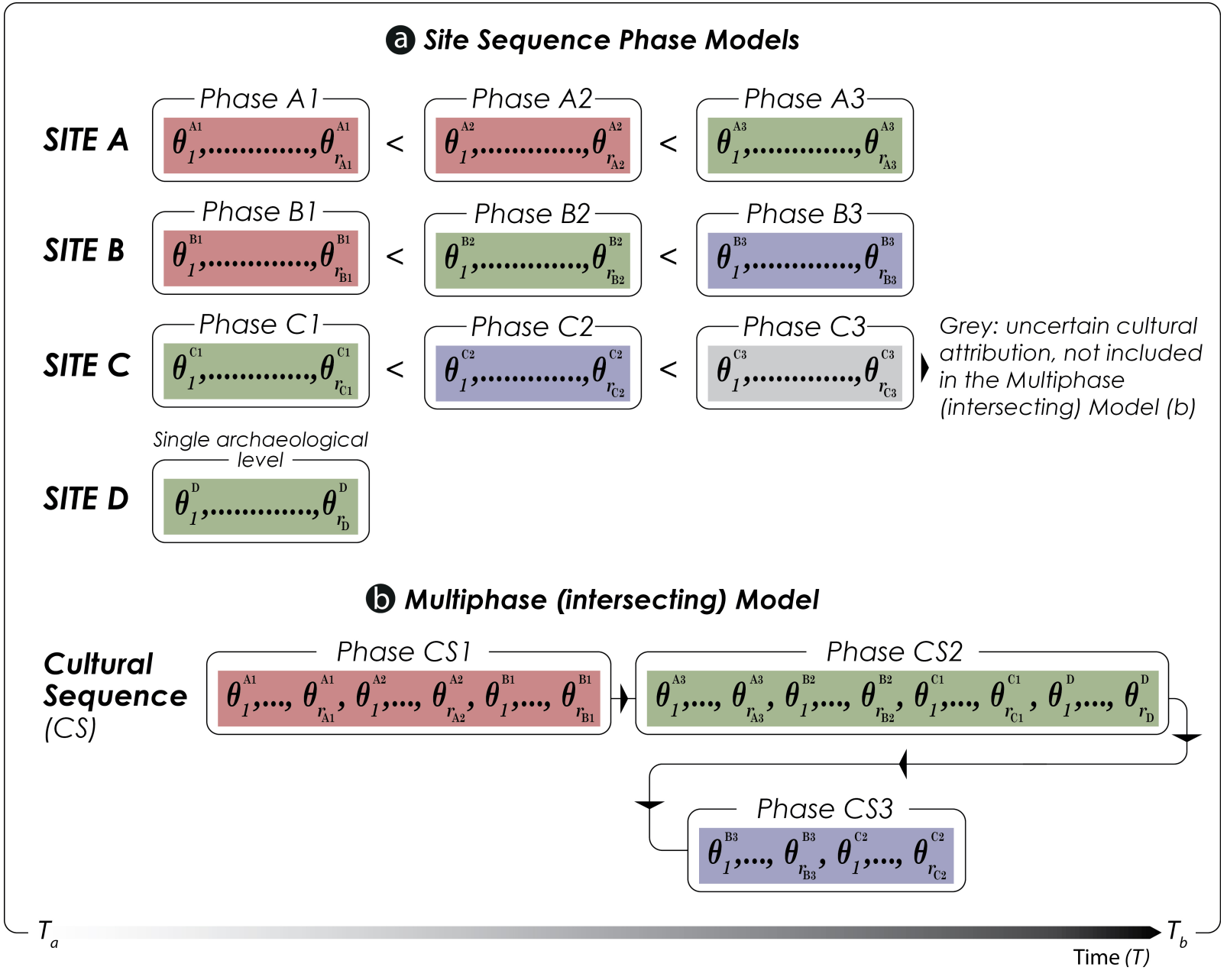
a Site Sequence Phase Models
SITE A
Phase A1
Phase A2
Phase A3
SITE B
Phase B1
Phase B2
Phase B3
SITE C
Phase C1
Phase C2
Phase C3
Grey: uncertain cultural attribution, not included in the Multiphase (intersecting) Model (b)
Single archaeological level
SITE D
b Multiphase (intersecting) Model
Cultural Sequence (CS)
Phase CS1
Phase CS2
Phase CS3
T_a
T_b
Time (T)

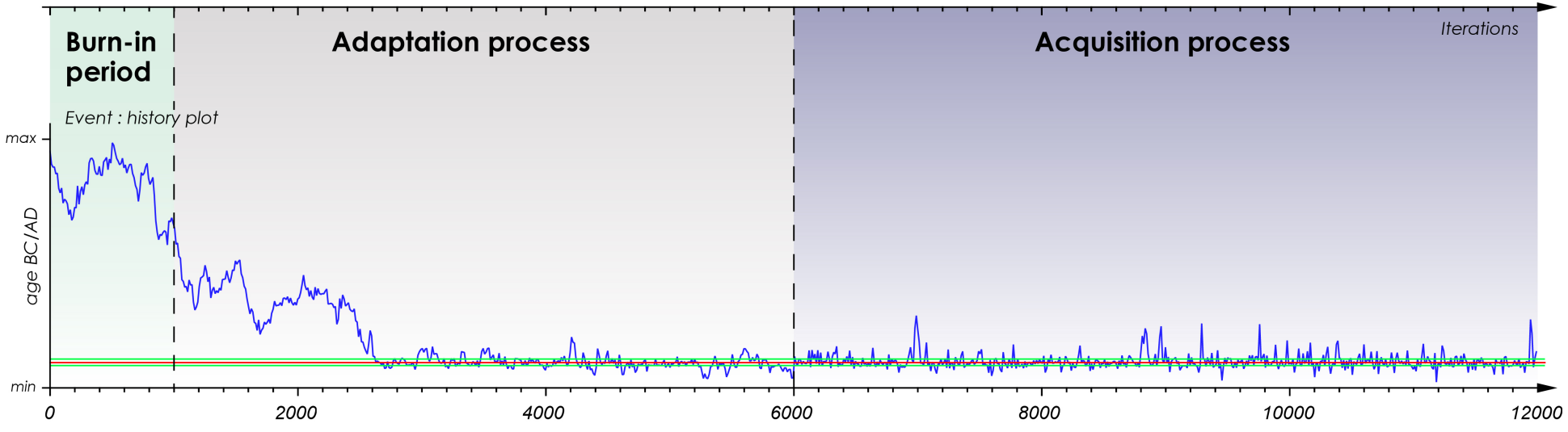
Burn-in period
Adaptation process
Acquisition process
Iterations
Event : history plot
max
min
age BC/AD
0
2000
4000
6000
8000
10000
12000

Table 1:

Cultural Phase	**No. dated sites**	**No. ^{14}C ages**	**No. retained sites 1st gen. model†**	**No. retained ages 1st gen. model†**	**No. retained ages 2nd gen. model**
Badegoulian	28	110	10	31	30
Middle & Upper Solutrean	20	85	7	26	26
Lower Solutrean	10	30	1	3	3
Aurig. V / Protosolutrean	3	8	1	4	4
Final Gravettian	10	55	5	15	13
Recent Gravettian	8	32	6	24	19
Middle Gravettian	23	98	10	40	19
Total	**102**	**418**	**40**	**143**	**114**

Site Name ††	Level	Lab Code	Outlier	Age	Error	Unmodeled cal BP HPD (95%)†		Posterior event date HPD (95%)		Reference	Notes
						From	To	From	To		
Early Gravettian											
Le Flageolet I	VII	GifA-99083	Yes	28720	350	33618	31739	—	—	Rigaud et al. 2016	
Le Flageolet I	VII	GifA-98362		28230	290	32923	31398	33669	31358	Rigaud et al. 2016	
Havrincourt	N2	Beta-332604		28100	180	32548	31415	33112	31357	Antoine et al. 2014	
Havrincourt	N2	Beta-307416	Yes	27020	140	31258	30854	—	—	Antoine et al. 2014	
l'abri Pataud	5	OxA-21587		28150	290	32835	31351	33562	31337	Higham et al. 2011	
l'abri Pataud	5	OxA-21585		28180	270	32826	31392	33526	31354	Higham et al. 2011	
l'abri Pataud	5	OxA-21586		28230	290	32923	31398	33652	31359	Higham et al. 2011	
l'abri Pataud	5	OxA-21588		28250	280	32924	31422	33632	31373	Higham et al. 2011	
Pyrenees Middle Gravettian Noaillian											
Carane 3	*1.3*	*GifA-100404**		26490	390	31202	29777	—	—	Foucher et al. 2001	age not included in cultural phase since attribution is uncertain; eliminated from run 2.
Carane 3	1.2	GifA-99245	Yes	23710	270	28366	27418	—	—	Foucher et al. 2000	
Enlene	5	GifA-97306	Yes	27980	480	33082	31076	—	—	Foucher et al. 2011	age included in cultural phase only
Gargas	2-6bis	Ly-3863 (SacA-6559)		27920	220	32416	31243	31929	31149	Foucher et al. 2011	
Gargas	2-6	Ly-3891 (SacA-6557)	Yes	26340	200	31014	30134	—	—	Foucher et al. 2011	
Gargas	2-6	Ly-4617 (SacA-9678)	Yes	26240	300	30994	29731	—	—	Foucher et al. 2011	
Gargas	2-6	Ly-4615 (SacA-9676)	Yes	26220	310	30990	29695	—	—	Foucher et al. 2011	
Gargas	2-5	Ly-4616 (SacA-9677)		26440	380	31165	29754	31525	30618	Foucher et al. 2011	
Gargas	2-5	Ly-4501 (OxA)		27350	145	31437	31023	31505	30901	Foucher et al. 2011	
Gargas	2-4	Ly-3411 (GrA)	Yes	25090	110	29456	28823	—	—	Foucher et al. 2011	
Gargas	2-4	Ly-4618 (SacA-9679)	Yes	28140	380	33021	31245	—	—	Foucher et al. 2011	
Gargas	2-3	Ly-3409 (GrA)		26480	420	31220	29705	31111	30087	Foucher et al. 2011	
Gargas	2-3	Ly-3410 (GrA)		26380	120	30956	30412	31021	30287	Foucher et al. 2011	
Gargas	2-3	Ly-4500 (OxA)		26075	130	30758	29886	30963	30053	Foucher et al. 2011	
Gargas	2-3	Ly-3403 (GrA)		25920	130	30620	29702	30954	29985	Foucher et al. 2011	
Gargas	2-2	Ly-3408 (GrA)	Yes	26910	130	31199	30805	—	—	Foucher et al. 2011	
Gargas	2-2	Ly-3402 (GrA)		26260	130	30900	30243	30571	29751	Foucher et al. 2011	
Gargas	2-1	Ly-3401 (GrA)		25520	110	30066	29282	30153	29026	Foucher et al. 2011	
Gargas	2-1	Ly-3405 (GrA)		25700	120	30319	29472	30301	29129	Foucher et al. 2011	
Gargas	2-1	Ly-3406 (GrA)		25230	110	29583	28955	29805	28787	Foucher et al. 2011	
Gargas	2-1	Ly-3404 (GrA)		25030	110	29401	28764	29629	28663	Foucher et al. 2011	
Gargas	2-1	Ly-3864 (SacA-6560)		24960	160	29408	28650	29665	28612	Foucher et al. 2011	
Tarté	1c	Lyon-2105 (OxA)	Yes	28410	150	32875	31736	—	—	Foucher et al. 2011	
Tarté	1c	Lyon-2999 (OxA)		27180	150	31349	30931	31501	30839	Foucher et al. 2011	
Tarté	1b	Lyon-2104 (OxA)		26600	170	31095	30561	31187	30279	Foucher et al. 2011	
Northern Generic Middle Gravettian (Noaillian, Rayssian)											
Calan	NA1	GifA-100637		24950	230	29515	28533	29953	28560	unpublished	Noaillian; age included in cultural phase only
Le Facteur	11/10	OxA-595	Yes	25630	650	30979	28525	—	—	Mellars et al. 1987	Noaillian; age included in cultural phase only
Le Facteur	11/10	OxA-594	Yes	25450	650	30886	28330	—	—	Mellars et al. 1987	Noaillian; age included in cultural phase only
Le Facteur	11/10	OxA-583	Yes	24720	600	30179	27702	—	—	Mellars et al. 1987	Noaillian; age included in cultural phase only
Le Facteur	11/10	OxA-586	Yes	24690	600	30146	27680	—	—	Mellars et al. 1987	Noaillian; age included in cultural phase only
Le Facteur	11/10	OxA-585	Yes	24400	600	29723	27443	—	—	Mellars et al. 1987	Noaillian; age included in cultural phase only
Le Facteur	11/10	OxA-584	Yes	24210	500	29272	27480	—	—	Mellars et al. 1987	Noaillian; age included in cultural phase only
Le Flageolet I	V	GifA-99084		26890	280	31329	30621	31579	30282	Rigaud et al. 2016	level contains both Noaillian and Rayssian
Le Flageolet I	V	GifA-98364		26160	270	30925	29711	31400	29294	Rigaud et al. 2016	level contains both Noaillian and Rayssian
Le Flageolet I	V	OxA-447	Yes	25700	700	31055	28491	—	—	Rigaud et al. 2016	level contains both Noaillian and Rayssian
Le Flageolet I	V	OxA-597	Yes	24800	600	30258	27752	—	—	Rigaud et al. 2016	level contains both Noaillian and Rayssian
Grotte du Renne	V	OxA-21567	Yes	23070	210	27721	26976	—	—	Higham et al. 2010	Rayssian; age included in cultural phase only
Grotte du Renne	V	OxA-21568	Yes	23180	210	27759	27104	—	—	Higham et al. 2010	Rayssian; age included in cultural phase only
Pataud	4 lower	OxA-168	Yes	26900	1000	33114	28882	—	—	Gowlett et al. 1987	level contains both Noaillian and Rayssian
Pataud	4 upper	OxA-374	Yes	26300	900	31976	28426	—	—	Gowlett et al. 1987	level contains both Noaillian and Rayssian
Taillis des Coteaux	Vig	Ly-2642		24950	135	29359	28667	29666	28593	Primault et al. 2010	Rayssian

Recent Gravettian											
Le Blot	48-39	Ly-1340		24610	200	29087	28165	28995	27800	Delvigne 2016	
Le Blot	48-39	Ly-1339		22210	150	26925	26066	28051	26572	Delvigne 2016	
Le Blot	48-39	Ly-1338 (GrA-17336)		24640	120	28941	28389	28966	28101	Delvigne 2016	
Le Flageolet I	*IV*	*OxA-596**	Yes	23250	500	28377	26415	—	—	Rigaud et al. 2016	age not included in cultural phase since attribution is uncertain
Laugerie-Haute Ouest	B (11)	Wk-35651		23951	171	28403	27698	28640	27404	Verpoorte et al. 2019	c. 11 in Verpoorte et al.
Laugerie-Haute Ouest	B (11)	WK-35652		23244	155	27742	27249	27960	27029	Verpoorte et al. 2019	c. 11 in Verpoorte et al.
Laugerie-Haute Ouest	B (11)	Lyon-10361/SacA-33970		23760	170	28197	27559	28463	27285	Verpoorte et al. 2019	c. 11 in Verpoorte et al.
Laugerie-Haute Ouest	B (11)	Wk-35675		23948	168	28395	27698	28657	27402	Verpoorte et al. 2019	c. 11 in Verpoorte et al.
Pataud	3	OxA-686	Yes	24500	600	29856	27506	—	—	Gowlett et al. 1987	
Pataud	3	OxA-685	Yes	23200	500	28309	26350	—	—	Gowlett et al. 1987	
Pataud	3	OXA-599	Yes	21740	450	27097	25139	—	—	Gowlett et al. 1987	
Pataud	3	OxA-165**		24440	740	—	—	—	—	Gowlett et al. 1987	same sample as OxA-164 and OxA-163
Pataud	3	OxA-164**		24250	750	—	—	—	—	Gowlett et al. 1987	same sample as OxA-165 and OxA-163
Pataud	3	OxA-163**		23180	670	—	—	—	—	Gowlett et al. 1987	same sample as OxA-165 and OxA-164
Pataud	3	Cobined OxA-163, -164, -165		23900	414	28754	27385	28814	27110		
Peyrugues	22	Gif-7998	Yes	24800	500	30000	27816	—	—	Allard 2011	
Peyrugues	22	Ly-3598 (SacA-5536)		24200	190	28640	27841	28764	27774	Allard 2011	
Peyrugues	21B	Ly-3597		23510	180	27922	27392	28126	27433	Allard 2011	
Peyrugues	20A	Ly-3596		23150	170	27703	27143	27848	27227	Allard 2011	
Peyrugues	20	Ly-3595 (SacA-5533)		23520	180	27931	27397	27729	26964	Allard 2011	
Renancourt	single	Beta-306063	Yes	21890	90	26338	25901	—	—	Paris et al. 2013	age included in cultural phase only
Renancourt	single	OxA-7761/Ly-633		22360	240	27199	26096	28074	26614	Fagnart et al. 2013	age included in cultural phase only
Renancourt	single	Lyon-9943 (SacA 32189)		22600	170	27326	26473	27849	26657	Paris et al. 2017	age included in cultural phase only
Renancourt	single	OxA-7654/Ly-632		23040	220	27717	26882	28018	26801	Fagnart et al. 2013	age included in cultural phase only
Renancourt	single	Lyon-11659 (SacA 39279)		23250	210	27794	27166	28056	26947	Paris et al. 2017	age included in cultural phase only
Renancourt	single	Lyon-9942 (SacA 32188)		23580	180	27989	27427	28254	27180	Paris et al. 2017	age included in cultural phase only
Final Gravettian											
Le Blot	32-22	Ly-1648		21870	230	26632	25705	26794	25898	Surmely and Hays 2011	
Le Blot	32-22	Ly-1647	Yes	20810	140	25477	24586	—	—	Surmely and Hays 2011	
Le Blot	32-22	Ly-1646		22190	220	27033	25991	26945	25972	Surmely and Hays 2011	
Le Blot	32-22	Ly-1645		22030	230	26876	25843	26875	25935	Surmely and Hays 2011	
Le Blot	32-22	Ly-1644		21510	220	26162	25346	26689	25828	Surmely and Hays 2011	
Le Blot	32-22	Ly-1643		21330	210	25997	25220	26737	25813	Surmely and Hays 2011	
Casserole	10b	Ly-9946		21810	150	26377	25783	26608	25876	Lenoble and Cosgrove 2012	
Pataud	2	OxA-162	Yes	22000	600	27483	25131	—	—	Gowlett et al. 1987	
Pataud	2	GrA-45013		21800	90	26208	25842	26458	25874	Nespoulet et al. 2013	
Pataud	2	GrA-45133		21910	90	26364	25915	26552	25911	Nespoulet et al. 2013	
Pataud	2	GrA-45132		22360	90	27028	26308	26993	26122	Nespoulet et al. 2013	
Pataud	2	GrA-45016		22470	90	27118	26471	27049	26201	Nespoulet et al. 2013	
Peyrugues	18	GifA-96224		22750	250	27520	26464	27095	26126	Allard 2011	
Peyrugues	18	GifA-92169		22400	280	27281	26082	27025	26051	Allard 2011	
Roches d'Abilly	single	OxA-22343		22170	140	26815	26033	26863	25987	Aubry et al. 2014	age included in cultural phase only
Aurignacian V/Protosol.											
Laugerie Haute Ouest	D (10)	WK-35654		22087	109	26594	26026	26154	25484	Verpoorte et al. 2019	
Laugerie Haute Ouest	D (10)	WK-35653		21837	140	26385	25816	26123	25535	Verpoorte et al. 2019	
Laugerie Haute Ouest	D (10)	Wk-35655		22028	138	26584	25953	26143	25486	Verpoorte et al. 2019	
Laugerie Haute Ouest	D (10)	Wk-35656		21865	112	26353	25864	26129	25551	Verpoorte et al. 2019	
Laugerie Haute Ouest	*E (9)*	*WK-35673**		21071	97	25660	25170	25740	25035	Verpoorte et al. 2019	age included only in sequence portion of model since level is sterile
Peyrugues	*14*	*GifA-95474**		21700	250	26499	25512	26576	25049	Allard et al. 1996	age included only in sequence portion of model since cultural attribution is uncertain

Lower Solutrean										
Laugerie Haute Ouest	H'	GifA-100632		20690	210	25465	24363	25416	24250	Roque et al. 2001	Burned bone but necessary to include since only dated sequence with Lower Solutrean age
Laugerie Haute Ouest	H'	Lyon-1175 (OxA)		20360	160	25013	24064	25196	24105	Roque et al. 2001	Burned bone but necessary to include since only dated sequence with Lower Solutrean age
Laugerie Haute Ouest	H' (8)	Wk-35667		20008	109	24358	23779	24925	23966	Verpoorte et al. 2019	
Middle Solutrean											These ages are placed in a single "Middle & Upper Solutrean" phase
Laugerie Haute Ouest	H''	Lyon-1174 (OxA)		20195	265	25057	23667	24455	23639	Roque et al. 2001	Burned bone but necessary to include since only dated sequence with Midde Solutrean age
Laugerie Haute Ouest	H'' (6)	Wk-35671		19606	74	23890	23368	24219	23530	Verpoorte et al. 2019	
Ormesson	sond. 29	Erl-17854		19096	121	23393	22646	23717	22827	Bodu et al. 2014	also known as Les Bossats
Upper Solutrean											These ages are placed in a single "Middle & Upper Solutrean" phase
Casserole	7b	Ly-9944		19300	120	23572	22923	23878	22967	Lenoble and Cosgrove 2012	
Casserole	7	Ly-9945		19020	110	23247	22555	23370	22833	Lenoble and Cosgrove 2012	
Cuzoul de Vers	31-29	Ly-10354 (SacA-33963)		19320	100	23559	22971	23775	22906	Ducasse et al. 2014	
Cuzoul de Vers	31-29	Ly-10352 (SacA-33961)		19380	100	23624	23020	23839	22931	Ducasse et al. 2014	
Cuzoul de Vers	31-29	Lyon-10353 (SacA-33962)		19050	100	23290	22609	23643	22809	Ducasse et al. 2014	
Cuzoul de Vers	31-29	Lyon 1682 (OxA-11220)		19510	110	23827	23127	24006	22994	Oberlin and Valladas 2012	
Cuzoul de Vers	31-29	Ly-10351 (SacA-33960)		19410	100	23660	23043	23875	22939	Ducasse et al. 2014	
Laugerie Haute Ouest	H''' (4)	Wk-35666		19676	112	24010	23396	23937	23133	Verpoorte et al. 2019	
Laugerie Haute Ouest	H'''	GifA-100630		19600	200	24065	23072	23894	22978	Roque et al. 2001	Burned bone but consistent with non-burned sample so included
Laugerie Haute Ouest	H'''	GifA-100634		19550	340	24306	22727	23884	22918	Roque et al. 2001	
Laugerie Haute Ouest	H'''	Ly-1173 (OxA)		19525	155	23918	23077	23859	22990	Roque et al. 2001	Burned bone but consistent with non-burned sample so included
Laugerie Haute Ouest	H''' (4)	Wk-39841		19388	103	23637	23021	23733	22964	Verpoorte et al. 2019	
Petit-Cloup-Barrat	8a2	Lyon-5604(SacA-12680)		19240	150	23578	22791	23823	22861	Ducasse et al. 2011	
Rochefort	4.3 - 4.2	GrA-39337		19025	120	23283	22552	23692	22808	Hinguant and Colleter 2010	Middle or Upper Solutrean attribution is uncertain.
Rochefort	4.3 - 4.2	GrA-39323		19190	110	23468	22821	23717	22855	Hinguant and Colleter 2010	Middle or Upper Solutrean attribution is uncertain.
Rochefort	4.3 - 4.2	GrA-38157		19500	70	23741	23185	23933	23042	Hinguant and Colleter 2010	Middle or Upper Solutrean attribution is uncertain.
Rochefort	4.3 - 4.2	GrA-38159		19600	80	23895	23350	24077	23147	Hinguant and Colleter 2010	Middle or Upper Solutrean attribution is uncertain.
Rochefort	4.3 - 4.2	GrA-34092		19320	90	23545	22984	23752	22912	Hinguant and Colleter 2010	Middle or Upper Solutrean attribution is uncertain.
Rochefort	4.3 - 4.2	GrA-34087		19490	90	23757	23131	23956	23003	Hinguant and Colleter 2010	Middle or Upper Solutrean attribution is uncertain.
Rochefort	4.3 - 4.2	GrA-34079		19590	90	23905	23315	24071	23116	Hinguant and Colleter 2010	Middle or Upper Solutrean attribution is uncertain.
Rochefort	4.3 - 4.2	GrA-34093		19600	90	23914	23332	24081	23130	Hinguant and Colleter 2010	Middle or Upper Solutrean attribution is uncertain.
Rochefort	4.3 - 4.2	GrA-34080		20090	100	24420	23893	24433	23586	Hinguant and Colleter 2010	Middle or Upper Solutrean attribution is uncertain.
Solutré	I11 c.3	CAMS-36630		19720	70	23990	23514	24155	23313	Montet-White et al. 2002	
Taillis les Coteaux	*Vib*	*Lyon 2640**		20870	105	25534	24811	25920	24367	Primault et al. 2010	age not included in cultural phase since attribution is uncertain
Badegoulian											
Le Blot	15	Lyon-1337		18000	80	22055	21546	22302	21491	BANADORA	
Le Blot	9	Lyon-1336		17850	80	21868	21372	21908	21149	BANADORA	
Contrée Viallet	3	Beta-377947		17610	70	21547	21013	21791	20881	Lafarge 2014	age included in cultural phase only
Contrée Viallet	3	Beta-377948		17600	70	21533	21003	21766	20884	Lafarge 2014	age included in cultural phase only
Cottier	II	Beta-377946		17910	70	21908	21466	22166	21238	Lafarge 2014	age included in cultural phase only
Cuzoul de Vers	27	Lyon-9078 (SacA-28345)		19150	110	23439	22761	23082	22768	Ducasse et al. 2014	Lower Badegoulian - without raclettes
Cuzoul de Vers	22	OxA-10976 (Lyon-1678)		19280	120	23554	22905	23027	22682	Ducasse et al. 2014	Lower Badegoulian - without raclettes
Cuzoul de Vers	22	Lyon-9077 (SacA-28344)		18920	110	23062	22492	23006	22668	Ducasse et al. 2014	Lower Badegoulian - without raclettes
Cuzoul de Vers	21	Lyon-9075 (SacA-28342)		18860	110	22995	22463	22924	22589	Ducasse et al. 2014	
Cuzoul de Vers	19	Lyon-9076 (SacA-28343)		18590	110	22744	22217	22867	22525	Ducasse et al. 2014	
Cuzoul de Vers	18	OxA-11118 (Lyon-1681)		19020	110	23247	22555	22825	22480	Ducasse et al. 2014	
Cuzoul de Vers	16	OxA-10975 (Lyon-1677)	Yes	19800	190	24293	23375	—	—	Ducasse et al. 2014	
Cuzoul de Vers	15	OxA-24964		19180	110	23461	22807	22773	22368	Ducasse et al. 2014	
Cuzoul de Vers	15	OxA-10974 (Lyon-1676)		18730	110	22881	22384	22741	22376	Ducasse et al. 2014	
Cuzoul de Vers	6	Lyon-9074 (SacA-28341)**		18620	100	—	—	—	—	Ducasse et al. 2014	same sample as OxA-24963

Cuzoul de Vers	6	OxA-24963**	18660	100	—	—	—	—	Ducasse et al. 2014	same sample as Lyon-9074 (SacA-28341)
Cuzoul de Vers	6	Combined Lyon-9074, OxA-24963	18640	70	22682	22355	22638	22066	Ducasse et al. 2014	
Cuzoul de Vers	6	OxA-10955 (Lyon-1674)	18730	110	22881	22384	22683	21860	Ducasse et al. 2014	
Lassac	locus 1 - c.2	Lyon-6417 (SacA-17494)	17400	110	21346	20679	21708	20743	Pétillon and Ducasse 2012	
Lassac	locus 1 - c.2	Lyon-6418 (SacA-17495)	17530	110	21527	20851	21807	20806	Pétillon and Ducasse 2012	
Pegourie	8c	Lyon-13122	18440	170	22630	21874	22887	21620	Ducasse et al. 2019	age included in cultural phase only
Pegourie	8b	Lyon-13121	17680	150	21811	20964	22116	20848	Ducasse et al. 2019	age included in cultural phase only
Petit-Cloup-Barrat	8a1	Lyon-3366 (Poz)	18595	150	22860	22099	22959	21849	Ducasse et al. 2011	
Rond du Barry	F2	Beta-297899	17490	80	21401	20860	21664	20804	Raynal et al. 2014	age included in cultural phase only
Rond du Barry	F2	Beta-297891	17510	70	21405	20899	21644	20828	Raynal et al. 2014	age included in cultural phase only
Rond du Barry	F2	Beta-297895	17680	70	21663	21101	21896	20937	Raynal et al. 2014	age included in cultural phase only
Rond du Barry	F2	Beta-306179	17720	80	21747	21151	21986	20958	Raynal et al. 2014	age included in cultural phase only
Oisy	4	Ly-6399 (SacA-17476)	18050	120	22236	21539	22528	21530	Debout et al. 2012	
Oisy	3	Ly-6398 (SacA-17475)	17810	110	21878	21225	21955	21031	Debout et al. 2012	
Oisy	3	Ly-4622 (SacA-9685)	17820	120	21902	21208	21970	21031	Debout et al. 2012	
Taillis des Coteaux	AG-V	Lyon-2639	18140	85	22278	21753	22513	21462	Primault et al. 2010	
Lower Magdalenian										
Fontgrasse	3	Erl-8926	16518	133	20259	19579	20812	19733	Bazile 2006	
Fontgrasse	3	Erl-8927	17100	144	21006	20238	21009	20138	Bazile 2006	
Fontgrasse	1a	Erl-8925	16838	143	20660	19958	20566	19055	Bazile 2006	
Fontgrasse	1a	Erl-8928	16338	153	20097	19324	20260	18972	Bazile 2006	
Gandil	ens. Inf.	GifA-96416	16980	170	20905	20052	21019	19689	Tisnerat Laborde et al. 1997	age included in cultural phase only
Gandil	ens. Inf.	GifA-96417	17480	180	21623	20634	21197	19747	Tisnerat Laborde et al. 1997	age included in cultural phase only
Gandil	ens. Inf.	GifA-97307	17290	180	21388	20418	21140	19845	Tisnerat Laborde et al. 1997	age included in cultural phase only
Gandil	ens. Inf.	Ly-2484 (Poz)	16538	144	20314	19581	20684	19218	Langlais et al. 2007	age included in cultural phase only
Gandil	ens. Inf.	Ly-2485 (Poz)	16507	144	20272	19554	20651	19168	Langlais et al. 2007	age included in cultural phase only
St. Germain	ens. Inf.	Lyon-10176 (SacA-32843)	16970	90	20712	20187	20899	19952	Barshay-Szmidt et al. 2016	age included in cultural phase only
St. Germain	ens. Inf.	Lyon-10232 (SacA-33707)	16900	80	20601	20129	20827	19900	Barshay-Szmidt et al. 2016	age included in cultural phase only
St. Germain	ens. Inf.	OxA-7260 (Ly-617)	16890	130	20688	20032	20923	19733	Lenoir et al. 1994	age included in cultural phase only
St. Germain	ens. Inf.	Lyon-10174 (SacA-32841)	16830	90	20542	20047	20777	19794	Barshay-Szmidt et al. 2016	age included in cultural phase only
St. Germain	ens. Inf.	Lyon-10231 (SacA-33706)	16670	80	20364	19878	20609	19598	Barshay-Szmidt et al. 2016	age included in cultural phase only
St. Germain	ens. Inf.	Lyon-10230 (SacA-33705)	16620	80	20305	19803	20557	19523	Barshay-Szmidt et al. 2016	age included in cultural phase only
St. Germain	ens. Inf.	Lyon-10175 (SacA-32842)	16450	90	20083	19590	20390	19290	Barshay-Szmidt et al. 2016	age included in cultural phase only
Taillis des Coteaux	AG-IIIa	Ly-2264	16920	170	20835	19993	20998	19636	Primault et al. 2010	
Taillis des Coteaux	AG-IIIa	OxA-12180	17130	65	20878	20469	20974	20265	Primault et al. 2010	

† - IntCal13 (Reimer et al. 2013)

* - 14C age only included in site sequence portion of model.

Table 3

Typo-Technological Phase	1st generation model Modeled Interval (95%) Begin	End	2nd generation model Modeled Interval (95%) Begin	End	duration (yrs)
Lower Magdalenian*	21211	*17980**	21182	*17978**	—
Badegoulian	23097	20773	23090	20777	2313
Middle & Upper Solutrean	24471	22806	24470	22787	1683
Lower Solutrean	25394	24004	25402	24007	1395
Aurignacian V / Protosolutrean	26131	25333	26173	25371	802
Final Gravettian	27030	25742	27126	25810	1316
Recent Gravettian	28771	26516	28973	26655	2318
Middle Gravettian (north of Pyrenees)	31974	28182	31520	28589	2931
Middle Gravettian Pyrenees	32169	28246	31925	28614	3311
Lower Gravettian*	*35599**	31245	*34990**	31245	—